UNIVERSITÀ DEGLI STUDI DI MILANO
FACOLTÀ DI SCIENZE MATEMATICHE,
FISICHE E NATURALI

Dipartimento di Scienze Biomolecolari e Biotecnologie
Scuola di Dottorato in Scienze Biologiche e Biomolecolari

Dottorato di ricerca in Biologia Cellulare e Molecolare
(CICLO XXIII)

Ferredoxin-NADP$^+$ reductase of *Plasmodium falciparum* (PfFNR): protein engineering and inhibition studies

Tesi di Dottorato di:
Danila CROBU

TUTOR: PROF. A. Aliverti
COORDINATORE DEL DOTTORATO: PROF. M. Bolognesi

ANNO ACCADEMICO 2009/2010

INDEX

SUMMARY

Malaria is recognised as one of the main health priorities by the World Health Organization. The most severe form of the disease, tropical malaria, is caused by *Plasmodium falciparum*. The diffusion of strains of this pathogen, resistant to traditional antimalarial treatments, urgently imposes the development of new therapies. *P. falciparum* belongs to the phylum Apicomplexa, which consists of unicellular, obligate intracellular parasites. These organisms possess an organelle of algal origin, the apicoplast, which has been shown to be required for pathogen survival and represents a known site of action of antimalarial compounds. In the apicoplast of *P. falciparum* a ferredoxin-$NADP^+$ reductase (PfFNR) has been identified. This enzyme is directly involved in the electron transfer pathway from NADPH to LytB which catalyzes the last step of the mevalonate-independent isoprenoid biosynthesis. The crystallographic structure of PfFNR in complex with the substrate analogue 2'-P-AMP showed the presence of two basic residues, His286 and Lys249, in the NADP(H)-binding site, which are conserved within the *Plasmodium* genus but not in other plant-type homologues.

Aim of this work has been to clarify the role of His286 and Lys249 in substrate binding and catalysis, and to identify and characterize PfFNR inhibitors.

The study of His286 and Lys249 was carried out by site-directed mutagenesis. The replacement of His286 resulted in a multifaceted effect, which highly depended on the replacement made. Steady-state kinetics showed that the substitution with aliphatic residues, i.e. Ala and Leu, decreases both k_{cat}/K_m^{NADPH} and k_{cat} indicating that His286 plays a critical role not only in NADP(H) binding but also in catalysis. 2'-P-AMP inhibition studies and titrations with $NADP^+$ also support this conclusions showing a decreasing in substrate affinity. Moreover rapid kinetic studies clearly demonstrated that the substitution His286Leu leads to a 3.4-fold decrease in the hydride-transfer (HT) rate between NADP(H) and FAD, with a destabilization of CT complexes between them. The His286Lys mutation resulted in the lowest k_{cat} but surprisingly this enzyme form binds 2'-P-AMP and $NADP^+$ with high affinity, indicating that this mutation destabilized the HT-competent conformation of the substrate NADP(H). Unexpectedly, steady-state kinetics and stopped-flow experiments showed that the mutation to Gln gave an enzyme more active than the wild-type, providing a better stabilization of the HT-competent

conformation between nicotinamide and isoalloxazine ring. Thus, His286 has a role in modulating the enzyme affinity for NADP(H) and in the precise positioning of the nicotinamide ring in the active site. The replacement of Lys249 with an Ala resulted in an enzyme form with a 10-fold decrease in K_m^{NADPH} and K_d for $NADP^+$ or 2'-P-AMP. In particular, as came out from the study of the NADH-$K_3Fe(CN)_6$ reductase reaction, this residue participates in substrate recognition by interacting with the 2'-phosphate of the pyridine dinucleotide.

By the *in silico* screening of two virtual libraries I have identified a pool of compounds potentially active against PfFNR. Five compounds, i.e. I8, I19, I21, I24 and I27, showed an IC_{50} in the micromolar range and I deeply characterized their inhibition mechanism by steady-state kinetic studies, also evaluating their specificity. Although in the *in silico* screening the substrate-binding site of PfFNR was targeted for the selection of enzyme ligands, all the compounds found turned out to inhibit PfFNR by a mixed-type mechanism, and did not show the expected pure competitive behavior towards NADPH. Some of the inhibitors turned out to be very specific for Apicomplexan FNRs.

Inhibition studies were carried out also to characterize the mechanism of ebselen, a compound selected within the experimental of a library of more than thousand diverse compounds. Steady-state kinetic studies and spectrofluorimetric analysis showed that ebselen is able to inhibit PfFNR with a two-phases mechanism consisting of a rapid enzyme inactivation followed by a slow FAD release. The inactivation process resulted to be irreversible without any formation of an initial reversible enzyme-inhibitor complex. Moreover the inactivation constant is higher at pH 8.2 rather than at pH 7 consistently with a covalent modification of PfFNR sulphydrylic groups. I also found that FAD release in PfFNR-C99A-C284S is markedly slowed down, suggesting a critical role of the active-site Cys284 in ebselen inhibition mechanism. Nevertheless the mild effect of mutation Cys284Ser on inactivation process suggests that FAD release and inactivation processes involve the modification of different Cys residues.

The need of large amount of purified enzyme for in-depth functional and structural characterization and inhibition studies prompted us to find a new expression system for PfFNR, able to decrease the cost of protein purification. Thus, I developed an expression system for PfFNR-C99A based on the fusion with the yeast SUMO protein. The partial *in vivo* degradation of poly-His-SUMO-PfFNR-C99A prevented the obtainment of high expression levels. However, a procedure for the rapid and cheap isolation of the

recombinant protein was developed, representing an attractive alternative to the previous protocol.

The features of PfFNR highlighted by the studies here reported, point out that PfFNR could represent an attractive drug target, suitable for the development of novel antimalarial compounds.

INTRODUCTION

1.1 MALARIA

In 2008 the World Health Organization estimated that malaria inflicted acute illness on 243 million of people worldwide and led to an estimated 863.000 deaths, of which 89% were in the African region, followed by the Eastern Mediterranean (6%) and South-East Asia (5%) regions (Figure 1.1). The majority (85%) of deaths were in children under five years of age.

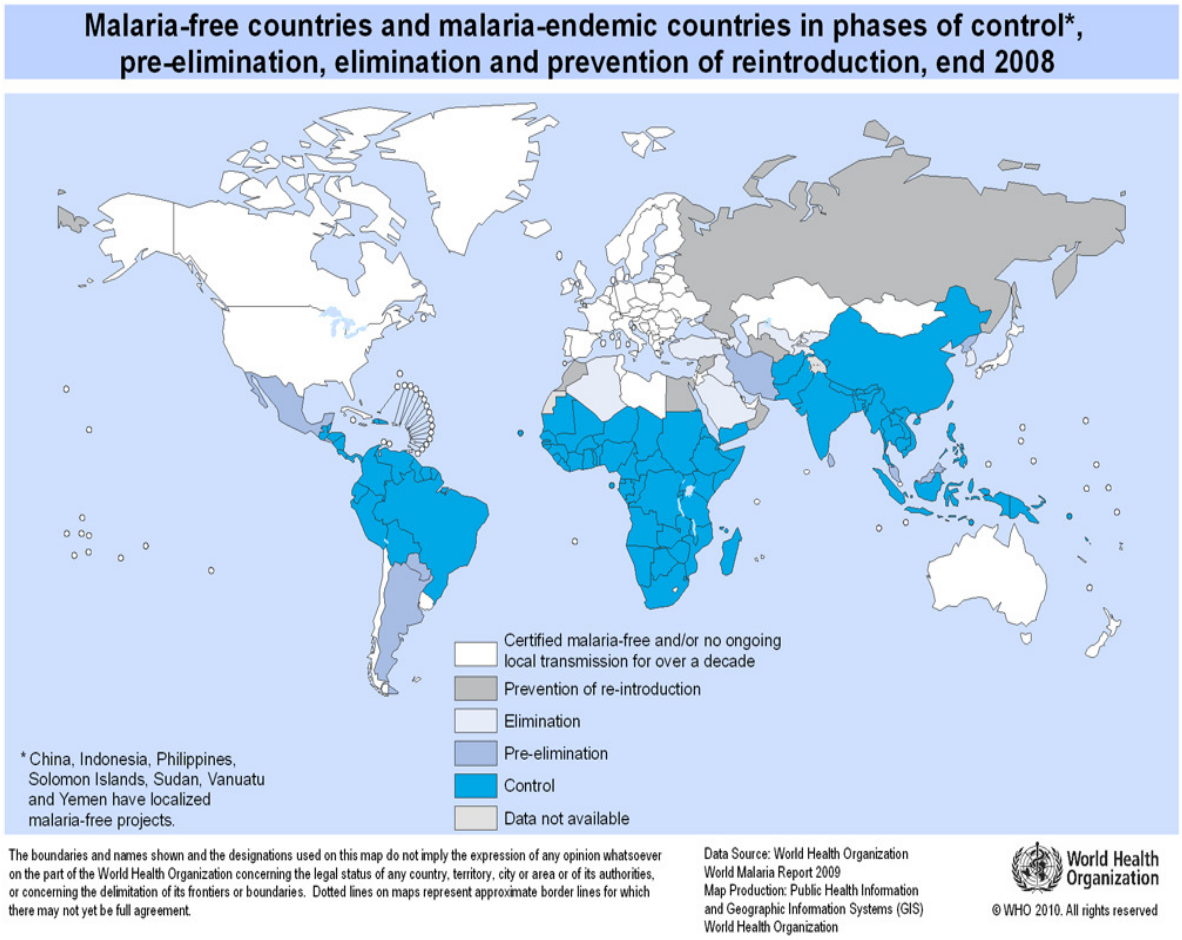

Figure 1.1. Worldwide malaria distribution.

Four *Plasmodium* spp. are responsible for malaria in humans: *P. vivax*, *P. malariae*, *P. ovale*, and *P. falciparum*. Malaria clinical manifestations are high fever, nausea and general weakening. The most severe form of the disease is cerebral malaria which presents

loss of consciousness, changes in mental status and coma, and, if not treated, is fatal within 24-72 hours. Cerebral malaria is caused by the infection of *P. falciparum*: parasitized red blood cells adhere to endothelial cells of brain and intestine causing blockage of the blood flow.

The emergence and spread of drug-resistant parasites made urgent the development of new antimalarial drugs. Currently, the two most widely used antimalarial drugs, chloroquine and sulfadoxine/pyrimethamine, are failing at an accelerating rate in most malaria-endemic regions. Moreover, other antimalarial drugs, such as the artemisinine derivatives, retain efficacy but have limitations, one of which is their high cost. Both the development of compounds against previously successfull targets and the identification of new target are required. The sequencing of *P. falciparum* genome revealed that the apicoplast, a vestigial plastid essential to parasite survival, may be a target for the development of new drugs.

1.2 THE *PLASMODIUM* PROTOZOAN

The phylum Apicomplexa includes many thousands of protozoan organisms and some of them, such as *Toxoplasma gondii*, *Cryptosporidium*, *Eimeria*, *Coccidia* and *Babesia*, are parasites which cause important clinical and veterinary diseases. *Plasmodium* belongs to Apicomplexa and it is the obligate intracellular parasite responsible for malaria (Seeber F. *et al*., 2008). All Apicomplexa differ from each other for transmission strategy and symptoms of the caused disease, but they share the same subcellular architecture (Roos D. S. *et al.,* 2002). Besides nucleus, mitochondrion and endoplasmic reticulum, Apicomplexa exhibit a distinctive 'apical complex' from which the phylum is named. This apical complex includes specialized secretory organelles (rhoptries, micronemes and dense granules) and cytoskeletal elements (Figure 1.2) which are involved in host cell attachment and invasion. In particular microneme proteins are secreted upon host cell contact, rhoptry contents are released concomitantly with the establishment of the intracellular parasitophorus vacuole, within which the replicating parasites reside (Carruthers V. B. *et al*, 1997), and dense granules are involved in the absorption of nutrients from host cell. Moreover the Apicomplexa possess an organelle, named apicoplast, related to non-photosyntetic plant plastid (McFadden G. I. *et al*., 1999, Fleige *et al.*, 2010).

Four *Plasmodium* species infect humans: *P. falciparum*, *P. vivax*, *P. ovale* and *P. malariae*. Their complex life cycle involves an insect vector (A*nopheles* mosquito) and a vertebrate

host (human). During a first exo-erythrocytic phase, the sporozoites reach the liver and invade the cells within which the asexual division starts. Then, thousands of merozoites are released from each liver cells and attach onto the red blood cell membrane entering them. Within the red blood cell, the asexual division starts giving new merozoites (erythrocytic phase). These merozoites are released by the lysis of the red blood cell and they immediately invade uninfected red cells. Some of the new merozoites in the red blood cells differentiate into male and female gametocytes. When A*nopheles* mosquito takes blood meal, also ingests gametocytes which continue their development in the mosquito giving sporozoites which reach the salivary gland (sporogonic cycle). Then mosquito during blood meal injects sporozoites in human blood stream and the cycle occurs again (Figure 1.3).

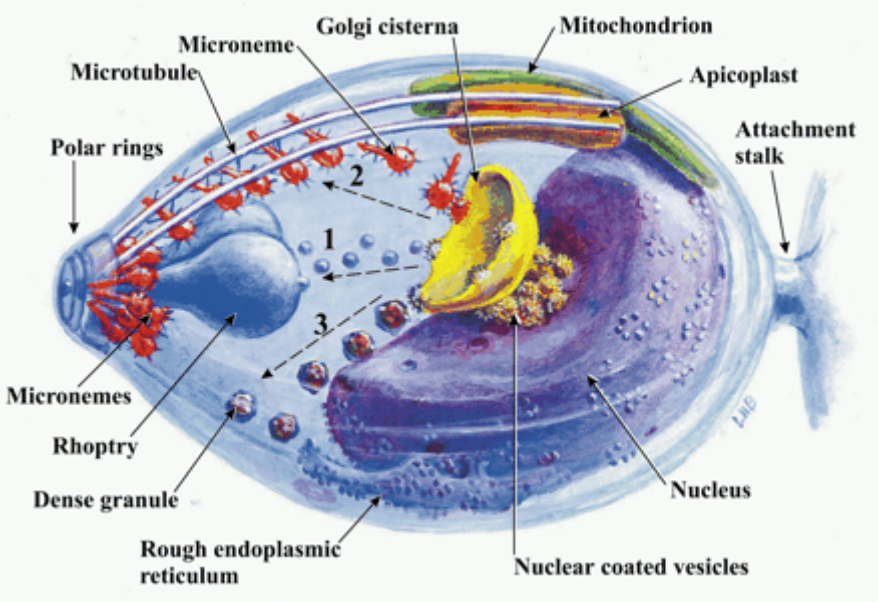

Figure 1.2. ***Plasmodium falciparum*** **structure. From Bannister L. H.** ***et al*****, 2003.**

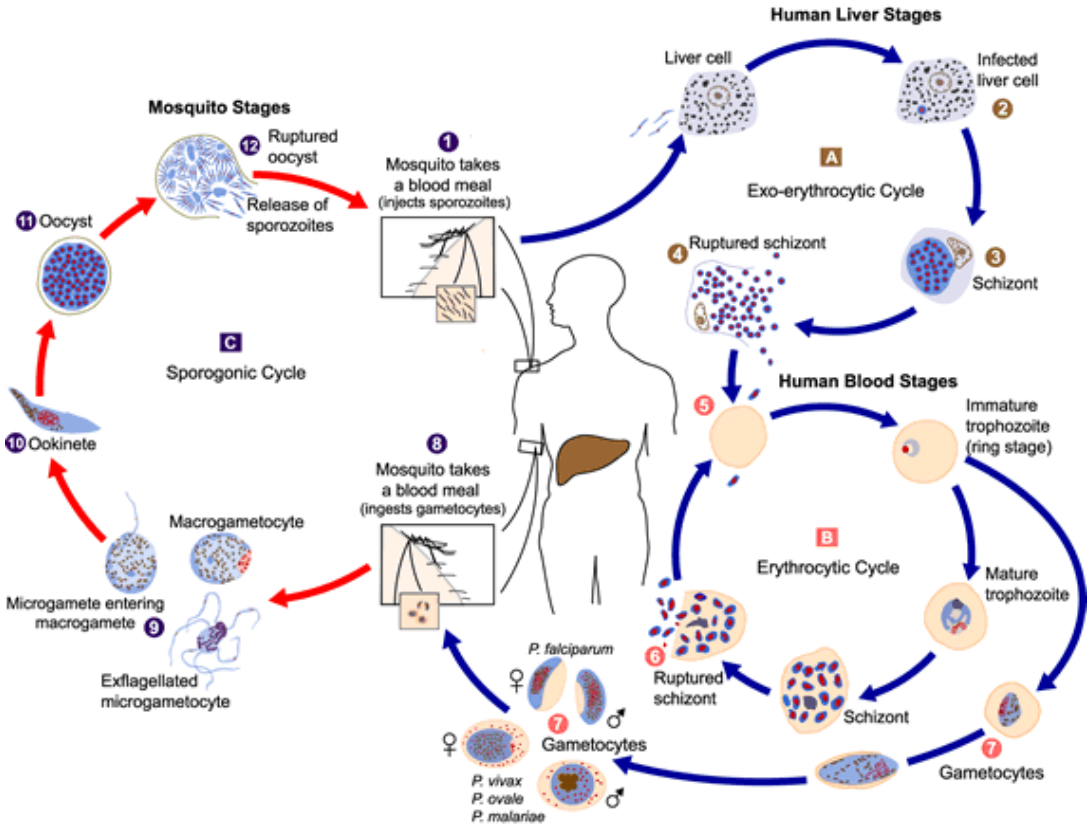

Figure 1.3. **Life cycle of *Plasmodium***

1.3 THE APICOPLAST

With the exception of *Cryptosporidium parvus* (Abrahamsen *et al*. 2004), Apicomplexan parasites possess a non-photosynthetic organelle, called apicoplast, which has an own genome with a size of 35 kb encoding two large-subunit and two small-subunit of ribosomal RNA, a complete set of tRNAs, ribosomal proteins, three subunits of RNA polymerase, a protein implicated in DNA replication, the elongation factor Tu, a *clp* protease and a few additional unknown ORFs (Wilson *et al.*, 1996, Funes *et al.*, 2004). Since the apicoplast is essential for parasite survival, its exclusive metabolic pathways are promising targets for the development of new drugs (Fleige *et al.*, 2010, Goodman *et al.*, 2007, Seeber *et al.*, 2010).

1.3.1 EVOLUTIONARY ORIGIN OF THE APICOPLAST

More than 50 years ago, morphological studies performed by electron microscopy on various apicomplexans, revealed the existence of a structure surrounded by four membranes (McFadden *et al.*, 1997, Siddall *et al.*, 1992). The discovery and then the sequencing of a circular 35 kb-extrachromosomal DNA element of *Plasmodium falciparum* encoding an RNA polymerase with high similarity to that of prokaryotes and chloroplast (Gardner *et al.,* 1991) were the first evidence for an alga-Apicomplexa connection. In particular the apicoplast genome analysis of *Plasmodium falciparum*, *Eimeria tonella* and *Toxoplasma gondii* strongly suggested that the apicoplast was originated by secondary endosymbiosis event in which an apicomplexan-like ancestor engulfed and retained another plastid-containing eukaryote (a photosynthetic unicellular alga), originated by a primary endosimbiosis between eukaryotic cell and photosynthetic prokaryote (Kolher *et al.*, 1997, Obornik *et al.*, 2009).

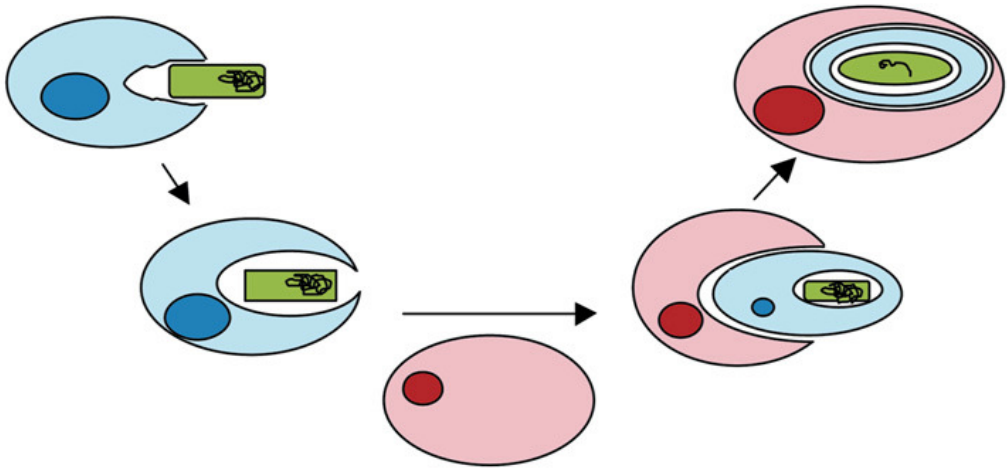

Figure 1.4. Evolutionary origin of the apicoplast. The photosynthetic prokaryote (green) is engulfed by a eukaryote (light blue) and some of the genes from the primary endosymbiont are transferred to the host nucleus (dark blue). Subsequently, this eukaryote containing the endosymbiont is engulfed further by a apicomplexan-like ancestor (pink). Here again, some genes are transferred to the host nucleus (red) reducing the apicoplast genome to the bare minimum. From Surolia *et al.*, 2004.

1.3.2 PROTEIN IMPORT INTO THE APICOPLAST

Throughout evolution, most of the genes coding for apicoplast-resident proteins have been transferred to the nuclear genome being synthetized on cytoplasmic ribosomes and then targeted to the organelle into the secretory pathway (Roos *et al.*, 1999, Yung *et al.*, 2003, DeRocher *et al.*, 2000). Soluble proteins are addressed to the apicoplast by a bipartite N-terminal sequence which is composed of a signal peptide (SP, 20-30 aminoacids,) followed by a transit peptide (TP, 50-200 aminoacids). The SP facilitates the entry of the protein into the secretory pathway. Here the SP is cleaved and thereby the following TP guides the protein toward the apicoplast and mediates its import. (Tonkin *et al.*, 2008, Sheiner *et al.*, 2008, Waller *et al.*, 2000). Inside the apicoplast the TP is then cleaved yielding the mature

polypeptide. The bipartite signal was exploited to perform bioinformatic predictions from the complete genome data of *P. falciparum*, leading to the identification of more than 500 putatively apicoplast-localized proteins. However, bioinformatic approaches provided a reconstruction of apicoplast metabolic pathways but only in few cases there are biochemical evidences supporting the bioinformatic prediction (Gardner *et al.*, 2002, Zuegge *et al.*, 2001). Probably, among these hundreds proteins only some of them are really localized in the apicoplast and some other have not been yet identified. The improvement of prediction tools based on the aminoacidic distribution on TP might help to identify candidate apicoplast-localized proteins (Zuegge *et al*., 2001, Foth *et al.,* 2003).

1.3.3 APICOPLAST FUNCTIONS

Since the evolutionary origin of the apicoplast, most of its metabolic pathways are fundamentally different from the mammalian host equivalents, making them potential targets for drug development. Using the metabolic pathways of plant chloroplast and bacteria as models, it has been illustrated an extensive apicoplast metabolic networks reconstructed from the list of apicoplast proteins that have been predicted using bioinformatics (Ralph *et al.,* 2004). It has been hypothesized that apicoplast is involved in the synthesis of iron-sulfur cluster, heme, fatty-acids, and isoprenoids.

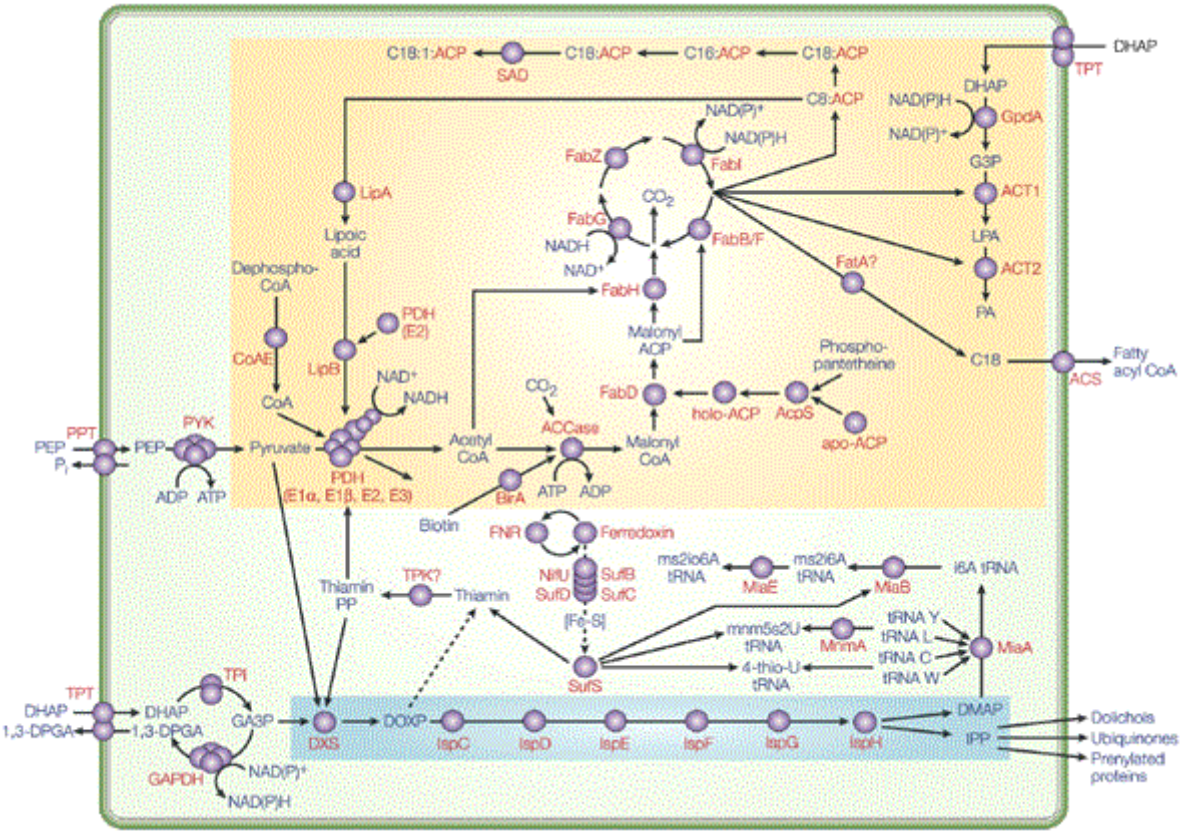

Figure 1.5. Overview of apicoplast metabolic pathways. From Ralph *et al.* 2004

1.3.3.1 FATTY-ACIDS SYNTHESIS

Fatty-acids (FA) synthesis has an important role in any living cell serving as building blocks of membrane lipids, for post-translational modifications of proteins etc. All the apicomplexan parasites have presumably an high demand for lipids and phospholipids since, in addition to the usual eukariotyc membrane-bound compartments (nucleus, endoplasmic reticulum, Golgi apparatus, mithocondria), they possess additional organelles such as micronemes, rhoptries, dense granules, the growing parasitophorous vacuole and the apicoplast (Bisanz *et al*, 2006). In all the Apicomplexa, enzymes of the FA synthesis have been found to be targeted in the apicoplast, which strong implicates that this organelle is the site of fatty-acids synthesis. The eukaryotic FA synthesis (type I) is carried out in one cytosolic multifunctional complex, the fatty-acid syntase which combines all enzymatic step of the synthesis. In contrast, the bacterial FA synthesis (type II) is carried out by distinct enzymes (Campbell *et al.*, 2001). In the apicoplast, an isoform of ACC (acetyl-CoA carboxylase) it has been found. This important enzyme catalyses the formation of malonyl-CoA from acetyl-CoA, the starting compound of FA synthesis. Moreover in the apicoplast enzymes FabH, FabZ, FabI and the protein ACP (acyl carrier protein) have been identified (Waller *et al.,*1998). Recently thiolactomycin, clodinafop and triclosan have been reported as compounds targeting enzymes of FA type II biosynthetic pathway. They are active against parasites either *in vivo* or *in vitro*. Thiolactomycin has been reported to kill parasites acting against FabH even if its target in *E.* coli is FabB (Rock *et al*., 2002, Heath *et al*., 2002). However the structural homology between the two enzymes explains this double inhibition.

Clodinafop is able to inhibit the plant-plastid ACC and it has been reported to inhibit the ACC of *T. gondii* (Jelenska *et al*., 2001). Triclosan is used as broad spectrum antibacterial in many consumer products and it has been recently shown that it inhibits FabI, the enzyme of *P. falciparum* and *T. gondi* which catalyses the NADH-dependent reduction of enoyl-ACP, either *in vivo* or *in vitro* (Levy *et al.*, 1999).

1.3.3.2 HEME BIOSYNTHESIS

In constrast with animals where heme biosynthesis is exclusively mitochondrial (Heinemann *et al.*, 2008), the pathway of heme synthesis in *P. falciparum* is a complex process involving different cellular compartments. Indeed, the initial step of the pathway is mithocondrial (Neuhaus *et al.*, 2000) but prediction tools indicate that some subsequent reactions take place in the apicoplast. Moreover, the steps of the pathway that follow apicoplast involvement seem to be either/both mithocondrial or cytosolic and probably the pathway terminates in mitochondrion. The evolutionary history of the apicoplast made probably this process complex and articulate. Maybe the redundance in the heme synthesis pathway of mitochondrion and apicoplast, subsequent to endosymbiosis, was resolved by the loss of several steps from each compartment, resulting in a chimeric pathway that is shared between several compartments. Notably, apicoplast and mithocondrion have an intimate physical association during specific stages of the parasite erythrocytic life cycle (Hopkins *et al.*, 1999) which could explain substrate exchange between compartments.
Heme synthesis is an established target for herbicides (Prasad *et al.*, 1995) and, since *P. falciparum* posseses plant-like heme synthesis enzymes, the elucidation of the entire pathway should provide further potential drug targets.

1.3.3.3 ISOPRENOIDS SYNTHESIS

Isoprenoids are a diverse range of compounds, composed of repeated isopentenyl pyrophosphate (IPP) units, and are important for organisms metabolism since participate to the formation of dolichols and ubiquinones, and to proteins prenylation. Two different metabolic pathways for the isoprenoids synthesis are known. One is the mevalonate-dependent pathway which is typical of eukaryotic cells. The other is the DOXP-pathway which was previously described only for bacteria and chloroplast (Schwender *et al.*, 1996, Disch *et al.*, 1998, Clastre M. *et al.*, 2007). In 1995 the first report of the existance, in *P. falciparum* apicoplast, of enzymes for DOXP-dependent IPP biosynthesis was published (Jomaa *et al.*, 1995). In the apicoplast the isoprenoids are synthetized starting from pyruvate and GA3P (glyceraldehyde 3-phosphate) which are converted in DOXP (1-

deoxy-D-xylulose-5-phosphate) by the enzyme DXS (DOXP synthase). This pathway is distinct from the eukaryotic biosynthesis of isoprenoids starting from mevalonate. On the basis of predicted apicoplast proteins, the enzymes involved in the DOXP-pathway have been identified in *P. falciparum* (Figure 1.5). After the formation of DOXP, there are six enzymes, called IspC/D/E/F/G/H, which provide the final products IPP and DMAP (dimethylallyl pyrophosphate). Even if the mechanism by which IPP is transported out of plastid is poorly understood, cytosolic enzymes using these compounds have been found. The isoprene units are used not only for protein prenylation, mithocondrial ubiquinones and dolichols formation, but also for the modification of tRNAs that are essential for apicoplast translation (Couto *et al.*, 1999). Drugs targeting the DOXP pathway (Jomaa *et al.*, 1995) might act by blocking the supply of any of the final products. Moreover given that the enzymes of the DOXP pathway are not found in humans, they constitute attractive candidate drug targets to combat the pathogens that rely on them (Singh *et al.*, 2007). In human clinical trials the use of fosfidomycin, an IspC inhibitor, demonstrates that this pathway is a potential drug target and gives impulse to found other targets in this pathway. In 2005 IspH (LytB), the enzyme which catalyses the last step of DOXP-pathway (Figure 1.6), has been proposed as new target of antimalarial drugs (Rohrich *et al.*, 2005).

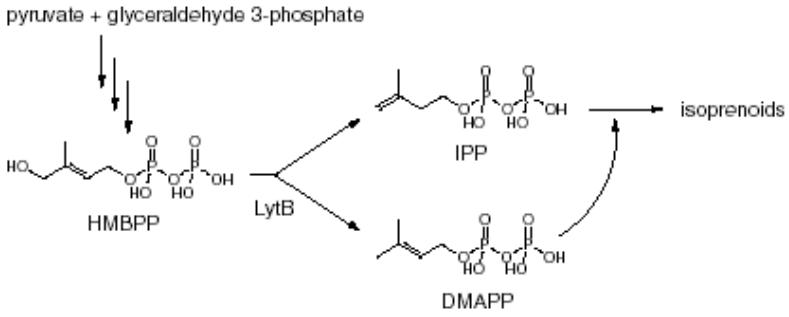

Figure 1.6: Reaction catalyzed by IspH (LytB). HMBPP ((*E*)-4-hydroxy-3-methyl-but-2-enyl diphosphate) is formed in several steps from pyruvate and glyceraldehyde 3-phosphate and then is converted into IPP and DMAP (dimethylallyl pyrophosphate).

Moreover LytB, which possesses a [4Fe-4S] cluster, was shown to directly interact with the NADPH-dependent electron transfer system of *P. falciparum* comprising a [2Fe-2S] ferredoxin (Fd) and ferredoxin-$NADP^+$ reductase (FNR). These two proteins are encoded in the nucleus and then translocated in the apicoplast (Vollmer *et al.*, 2001, Seeber *et al.*, 2005). Activity assays and mass spectrometry experiments demonstrated that the Fd/FNR

redox system is directly involved in a apicoplast metabolic pathway serving as an electron donor for LytB.

1.4 FERREDOXIN-NADP$^+$ REDUCTASE

Ferredoxin-NADP$^+$ reductase are flavoenzymes (FNR; EC 1.18.1.2) belonging to dehydrogenase electron-transferases and containing flavin adenine dinucleotide (FAD) as prosthetic group which is responsible of the catalytic properties of holoenzyme. FAD, derived from vitamin B_2, is characterized by the presence of isoalloxazine ring which represents the reactive portion. The flavin can exist in three different redox states, the oxidized, coloured of the characteristic bright yellow (FAD), the one-electron reduced semiquinoid and the fully reduced ($FADH_2$) species.

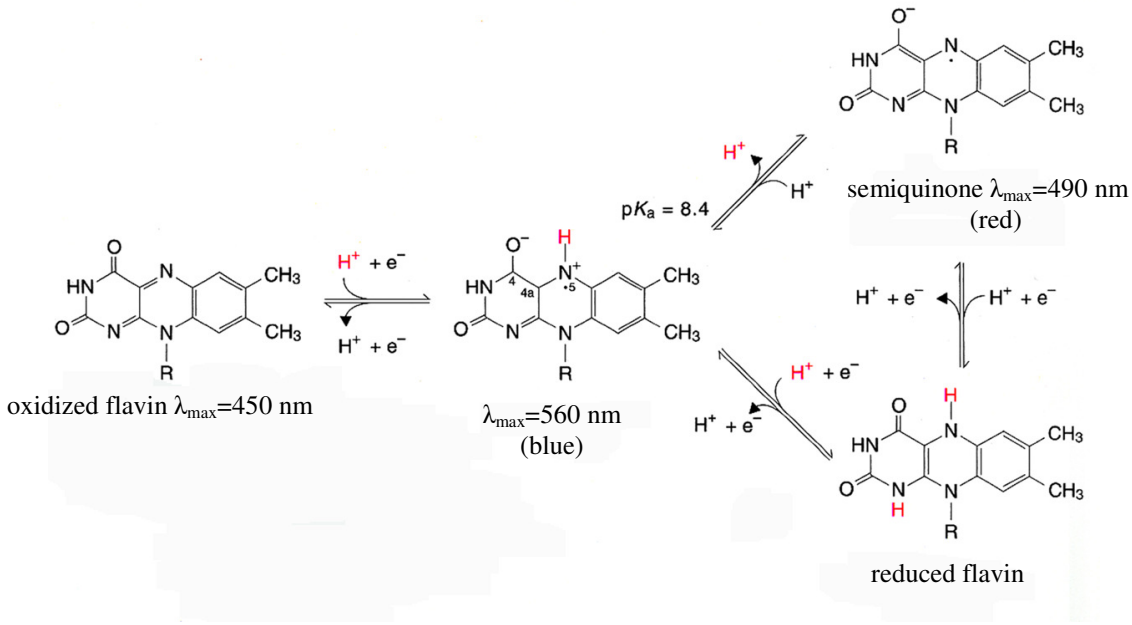

Figure 1.7. Redox states of flavin.

FNRs share the ability to catalyze the transfer of reducing equivalent between NADP(H) and ferredoxin (Fd), a protein containg Fe-S cluster, or flavodoxin (Fld), a protein containing FMN as prosthetic group.

$$2\ Fd\ (Fe^{+2}) + NADP^{+} + H^{+} \rightleftharpoons 2\ Fd\ (Fe^{+3}) + NADPH$$

$$2\ Fld\ (FMNH) + NADP^{+} + H^{+} \rightleftharpoons 2\ Fld\ (FMN) + NADPH$$

Flavoproteins with FNR activity have been found in plant plastids, bacteria and mithocondria. An event of convergent evolution originated two families of flavoproteins which exhibit different sequences and structures but catalyse the same reaction. The first is the family of mithocondrial-type FNRs, known as adrenodoxin reductases (AdRs), the second comprises plant-type FNRs.

1.4.1 PHOTOSYNTHETIC FNRs

In plant photosynthetic tissues, FNR is associated to thylakoids membrane where catalyses the last step of the electron transport chain. In particular it promotes the transfer of two electron from ferredoxin (one-electron donor, Fd), reduced by photosystem I, to $NADP^{+}$(two-electron acceptor)

$$2\ Fd_{red} + NADP^{+} + H^{+} \longrightarrow 2\ Fd_{ox} + NADPH$$

In 1984 Batie and Kamin formulated the first detailed pathway for the FNR-mediated electron transfer between ferredoxin and $NADP^{+}$. The overall reaction was interpreted as an ordered two-substrate process, with $NADP^{+}$ binding first. Moreover they demonstrated that the kinetics were consistent with the formation of ternary complexes as intermediates of the catalytic mechanism (Figure 1.8, step 2 and 5). FNR catalyses this reaction exploiting the capability of FAD to accept one electron from ferredoxin (one-electron donor) and to transfer two electron to $NADP^{+}$ (two-electron acceptor) as hydride ion.

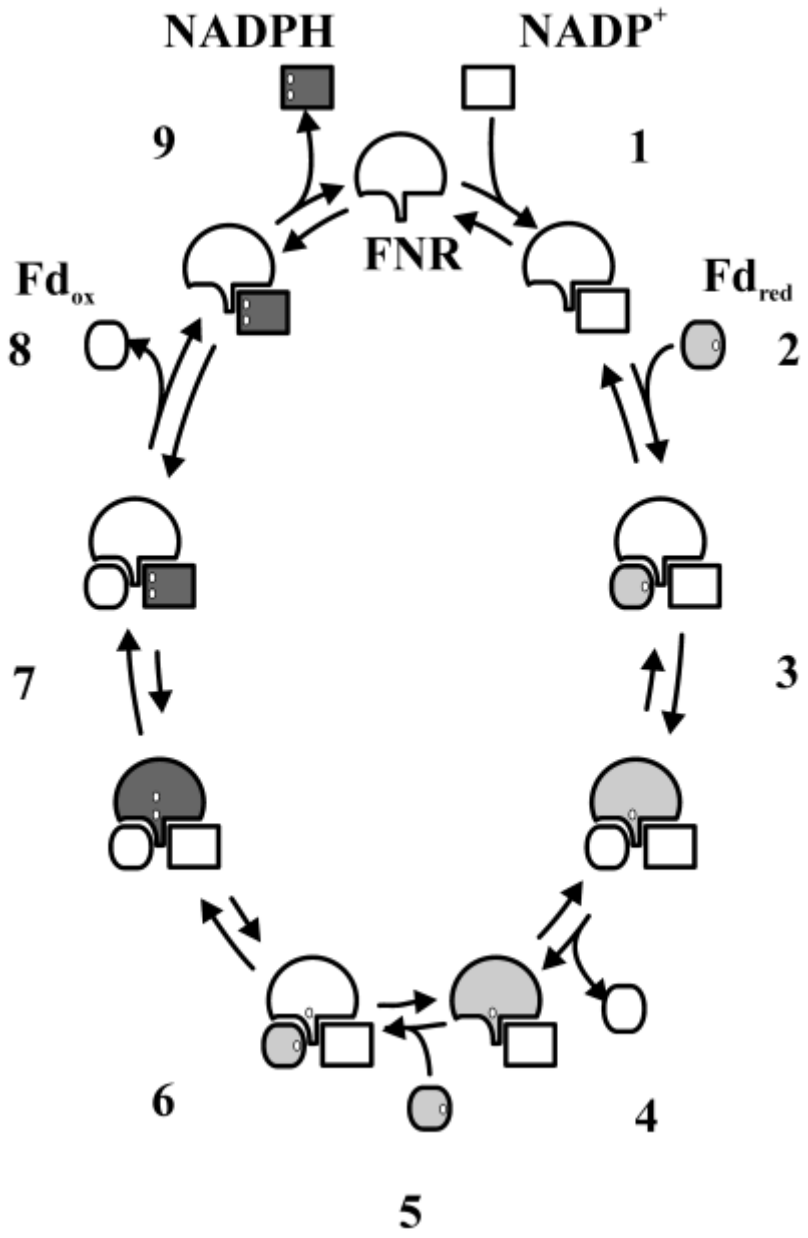

Figure 1.8. The electron transfer mechanism of FNR. Oxidized forms are white, one-electron reduced forms are light grey and two-electron reduced forms rea dark grey. From Carrillo *et al.,* 2003.

1.4.2 NON-PHOTOSYNTHETIC FNRs

In 1990 an FNR has been found in a non-photosynthetic plastid (Morigasaki, 1990). This isoform catalyses the electron transfer in an opposite direction respect to chloroplast FNR. In particular non-photosynthetic FNR transfers electrons from NADPH to ferredoxin:

$$2\ Fd_{ox} + NADPH \longrightarrow 2\ Fd_{red} + NADP^{+} + H^{+}$$

In plant roots, reduced ferredoxin acts as electron donor for enzymes involved in nitrogen and sulfur assimilation. Tissues from pea root have been shown to be able to induce, in presence of nitrates, synthesis of a protein detected by anti- leaf FNR (lFNR) antibodies (Bowsher *et al.*,1993). Moreover an FNR from root (rFNR) it has been isolated from a cDNA library of root tissues genes transcribed after nitrates exposure (Aoki, 1994, Ritchie *et al.*, 1994). This gene regulation is markedly different from that of photosynthetic FNRs which are regulated exclusively by light.

1.4.3 FNRs TRIDIMENSIONAL STRUCTURE

Today tridimensional structure of various plant-type FNRs (Karplus *et al.*, 1991; Karplus *et al.*, 1994; Deng *et al.*, 1999; Aliverti *et al.*, 2001), *Anabaena* FNR (Serre *et al.*, 1996), *E. coli* FNR (Ingelman *et al.*, 1997) *Azotobacter vinelandii* FNR (Prasad *et al.*, 1998) are known. Plant-type FNR is made of two structural domains, each containing approximately 150 amino acids. The C-terminal region, topologically similar to the supersecondary structure named Rossmann fold, includes most of the residues involved in NADP(H) binding. Plant-type FNRs are remarkably specific enzymes showing a strong preference for NADP(H) over NAD(H). Substrate discrimination is due to a number of charge interactions that FNR establishes with the 2'-phosphate group of the substrate (Carrillo *et al.,* 2003, Aliverti *et al.*, 2008). The N-terminal region comprises a six-stranded antiparallel β-barrel, a small β-sheet and an α-helix, and provides most of the residues involved in the FAD binding (Figure 1.9). The isoalloxazine ring of FAD is sandwiched between the aromatic side chain of two tyrosine residues. In 2001 the 1.7 Å resolution crystal structure of the recombinant corn root FNR has been shown to be very similar to the structures of ferredoxin–$NADP^{+}$ reductases from photosynthetic tissues (spinach leaf FNR). Only a

sligthly different conformation of a short N-terminal extension has been found being maybe responsible for the different affinity for ferredoxin isoforms in photosynthetic and non-photosynthetic FNRs (Aliverti *et al.,* 2001).

Figure 1.9. Ribbon representation of plant-type FNR. In blue FAD binding domain is shown. In pink NADP(H) binding domain is shown and FAD prosthetic group is shown in yellow.

1.5 FERREDOXIN-NADP$^+$ REDUCTASE OF *Plasmodium falciparum*

1.5.1 PRIMARY STRUCTURE

Ferredoxin-NADP$^+$ reductase of *Plasmodium falciparum* (PfFNR) is encoded in the nucleus and then translocated in the apicoplast through a bipartite N-terminal sequence. On the basis of sequence alignment with other FNRs, it has been determinated that mature PfFNR starts at Lys56 yielding a 36 kDa protein with 316 amino acids. A comparison between sequences of different isoforms of FNR shows an high similarity of PfFNR with plant-type homologues, in particular with the homologue in non-photosynthetic tissues (Figure 1.10). As *P. yoelii* and *P. knowlesi*, PfFNR has not Trp residues; Trp309, conserved in all FNR, is substituted with a Val. Despite the most conserved residues are in NADPH and FAD binding sites, some significant substitutions are present in PfFNR sequence (Figure 1.11). In the NADPH binding domain Arg235 is substituted with a Tyr and Lys244 with a Ser, reducing the number of positively charged residue. Leu274, a residue situated in the –CGLK- binding motif of NADPH, it is substituted with an His. In the –LYSIAS- binding motif of FAD Ala98 is substitued with a Ser and at position 114 a Cys, conserved in other FNRs, is substitued with an Ala. Similarly to Apicoplexa FNRs, PfFNR shows two insertions of 28 and 5 amino acids respectively. The larger insertion is situated in proximity of FAD binding domain, the shorter is localized after the –GTG- motif of NADP$^+$ binding. Moreover PfFNR posesses 6 cysteine residues, two of which are conserved in other FNRs (Cys132 and Cys272).

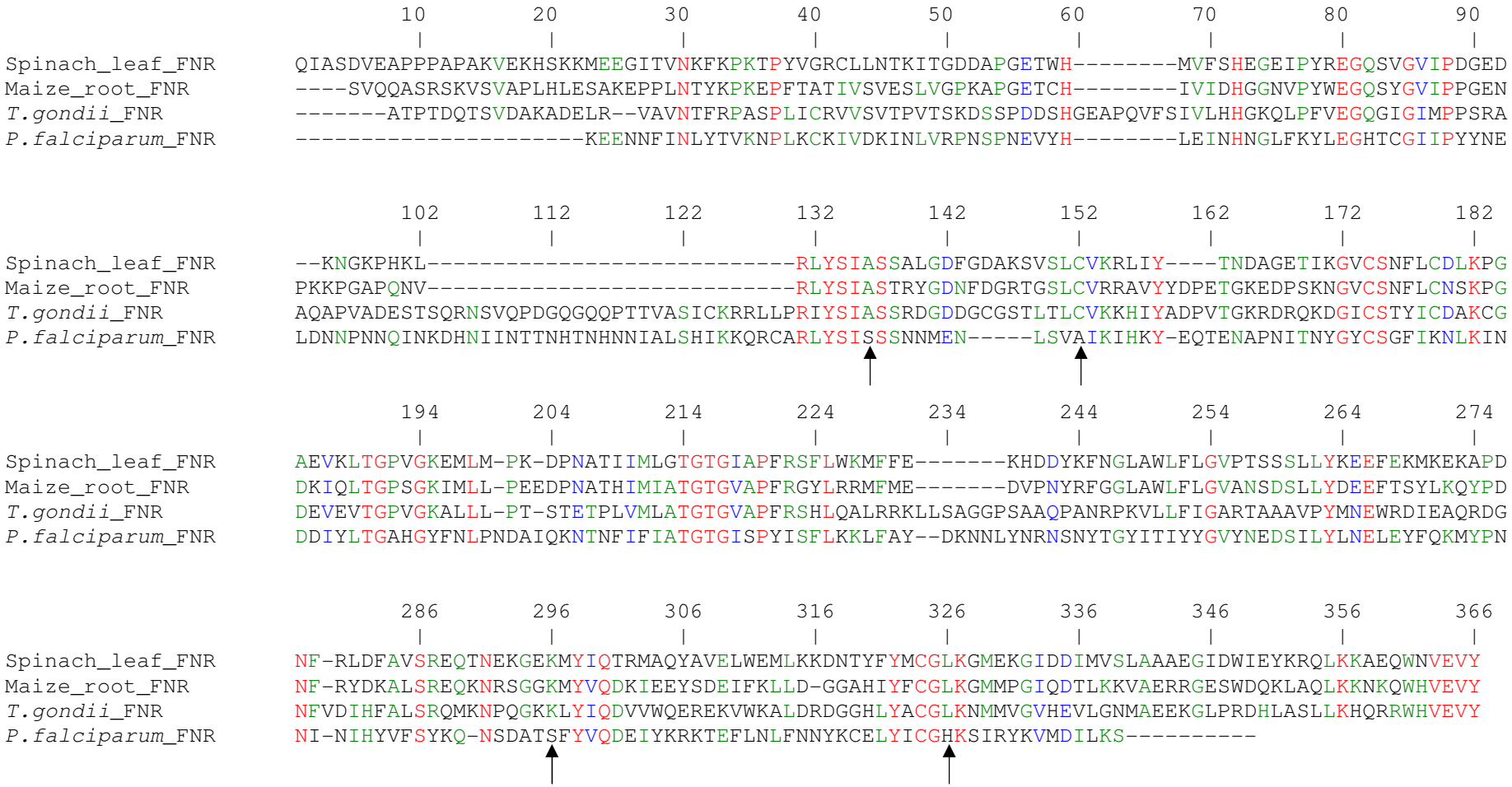

Figure 1.10: FNRs sequences alignment. Most conservative residues are shown in red, conservative substitutions are shown in green and in blue. Arrows indicate unconservative residues in the cofactors binding motifs.

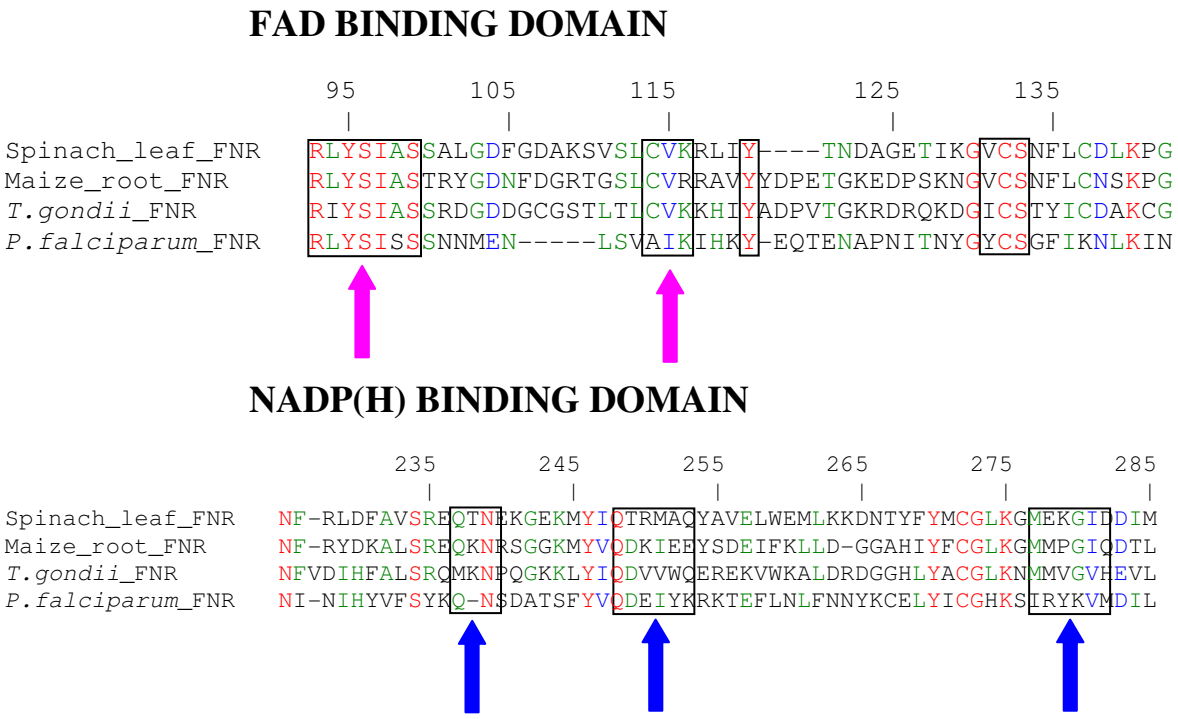

Figure 1.11: FAD and NADPH binding domains of FNRs. Numbering refers to spinach leaf FNR. Pink arrows indicate substitutions in FAD binding domain. Blue arrows indicate substitutions in NADPH binding domain.

1.5.2 TRIDIMENSIONAL STRUCTURE

In 2007 crystallographic structure of PfFNR both in its free form and in complex with 2'-P-AMP, an anologue of the substrate NADP(H), has been solved (Milani *et al.*, 2007). In both crystal forms PfFNR crystallized as dimer stabilized by a intermolecular disulfide bridge between the Cys99 of each subunit (Figure 1.12). As the other plant-type FNRs, PfFNR consists of two domains: the N-terminal FAD binding domain, comprising residue 1-160, and the C-terminal NADP(H) binding domain, built by residues 166-316. The FAD domain hosts a β-barrel built by two perpendicular three-stranded antiparallel β-sheets (β1β2β5 and β3 β4 β6) and a single α-helix (αA), nestled between β5 and β6. The C-terminal domain hosts a five-stranded parallel β-sheet (β9β8β10β11), surrounded by seven α-helices (αB-αH).

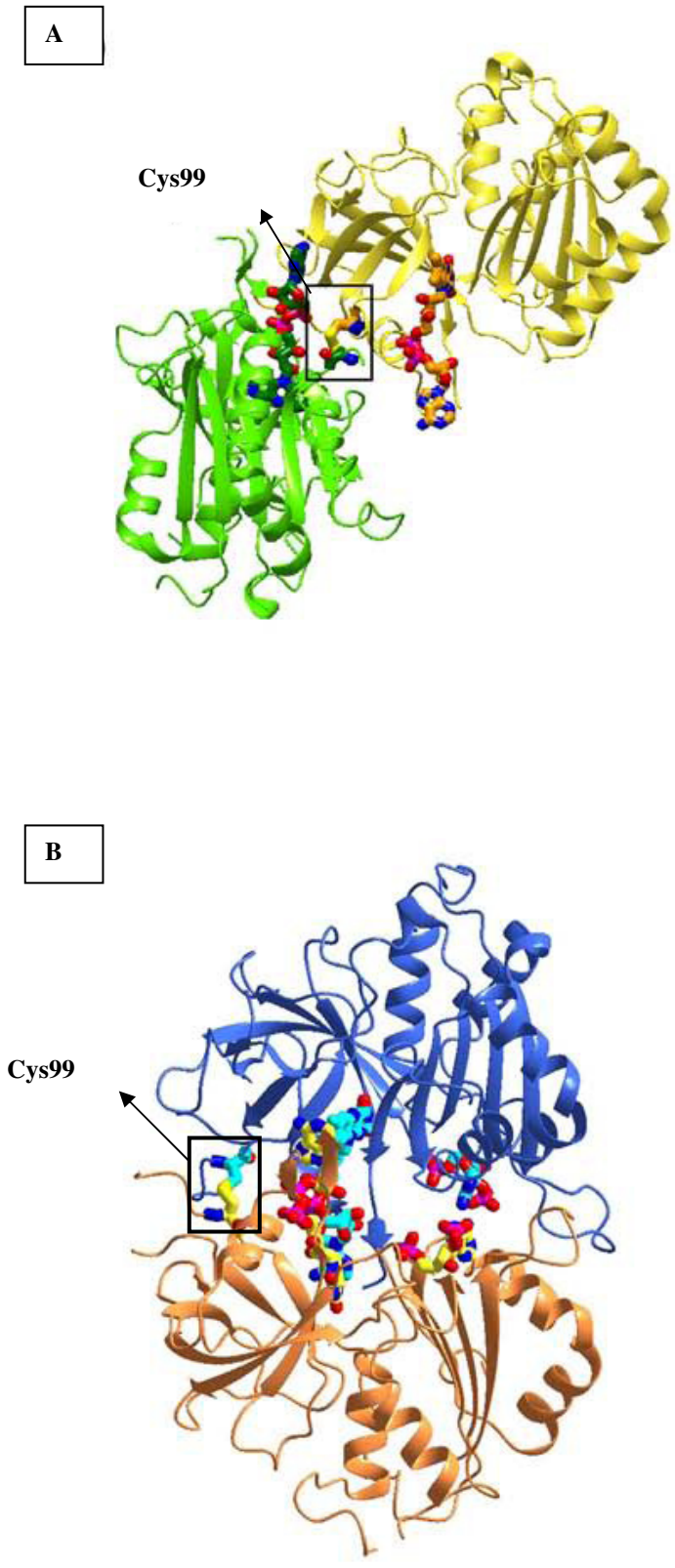

Figure 1.12. Tridimensional structure of PfFNR (A) and PfFNR/2'-P-AMP complex (B). In PfFNR/2'-P-AMP complex the two monomers adopt a very close conformation involving 2'-P-AMP binding site. Conversely, in the PfFNR free form contact area between the two monomers is around Cys99.

In both crystal forms PfFNR displays five disordered surface regions: the N-terminal residues 1-4, the long loop between β3 and β4 (residues 63-97), the β5- αA loop (residues 126-133), the αB-β9 loop (residues 196-205), and the αH- αI loop (residues 299-305).

The FAD molecule is observed essentially in the same extended conformation in both crystal forms. The isoalloxazine ring is hosted in a pocket between the two protein domains, sandwiched between the conserved C-terminal Tyr316 and four conserved amino acids residues of the β4 strand. The overall FAD binding mode described for PfFNR is essentially conserved in other plant-type FNRs, the main conformational differences affecting only the protein surface location of the cofactor's adenosine moiety. However given the location of the adenine ring far from the active site region, such structural variation should bear little relevance for PfFNR catalysis.

The most significative differences between PfFNR and other FNRs structure are located in the 2'-P-AMP binding site (Aliverti *et al.*, 2008). (i) The ligand interacts by hydrogen bond with two regions of the C-terminal domain (Ser247, Tyr258, Gln260, His286 and Ser288) and with Lys119 of the N-terminal domain. (ii) The negative charge of the 5'-phosphate is balanced by Lys119 and by His286, whereas there are no positevely charged residues balancing the negative charge of the 2'-phosphate. A compensation can be offer by Lys287 and/or Lys292 from the opposing subunit in the dimeric assembly, suggesting that the achievement of inter-molecular electrostatic balance at the 2'-phosphate might be one of the driving forces guiding PfFNR dimerization induced by 2'-P-AMP or by $NADP^+$. In SoFNR the 2'-phosphate charge is compensated intramolecularly by the highly conserved residues Arg235 (Tyr248 in PfFNR) and Lys244 (Ser256 in PfFNR). (iii) The 2'-P-AMP adenine moiety is sandwiched between Tyr258 and His286.

The mosts stricking differences between PfFNR structure in free form and in complex with 2'-P-AMP are located in the NADP(H) binding domain. As can be seen in Figure 1.13, both the β9-αF loop (residues 248-257) and the αH helix (residues 289-298) undergo notably structural transistions: in absence of 2'-P-AMP, the loop is shortened by seven residues while the helx is elongated by two turns and is shifted towards the FAD binding pocket by about 2 Å.

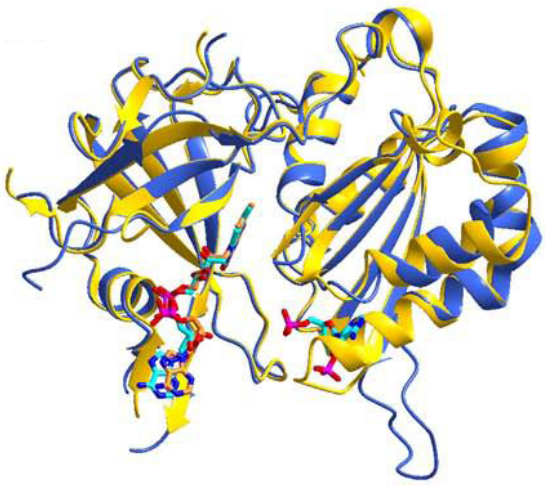

Figure 1.13. Structure of PfFNR (yellow ribbon) is overlaid on the structure of PfFNR/2'-PAMP complex (blue ribbon). The lower right part highlights the conformational helix-coil transition occurring at the β9-αF loop, in the NADP(H) binding domain in absence of 2'-P-AMP.

1.5.3 FUNCTIONAL PROPERTIES

In 2005 it has been demonstrated that the ferredoxin/ferredoxin-$NADP^+$ reductase redox system of *P. falciparum* serves as the physiological electron donor for LytB, the enzyme which catalyses the last step of the DOXP pathway of isoprenoids biosynthesis in apicoplast (Rohrich *et al.*, 2005). This results represents the first evidence of a direct involvement of PfFNR in apicoplast metabolism. An interesting feature of PfFNR, unique among plasmodial reductase, is its ability to undergo dimerization and this process is favoured by the presence of either 2'-P-AMP or $NADP^+$. Dimer relies on the oxidation of residue Cys99 in two opposing subunits and it has been found to be essentially inactive, but full activity is recovered upon disulfide reduction (Milani *et al.*, 2007, Balconi *et al.*, 2009). Similar regulatory mechanism has been observed in plant non-photosynthetic plastid where thioredoxins are held to play a central role in redox regulation (Balmer *et al.,* 2006). It has been suggested that two thioredoxins (Trx2 and Trx3) are apicoplast-resident,

based on the detection of a predicted signal peptide at the N-terminus (Nickel *et al.,* 2006). Apicoplast-resident thioredoxin would require a thioredoxin reductase (TrxR), but the TrxR in *P. falciparum* is cytosolic. Therefore, alternative redox regulators should be sought to prevent dimerization *in vivo*.

AIM OF THE PROJECT

Malaria is recognised as one of the major health priorities by the World Health Organization. The most severe form of the disease, tropical malaria, is caused by *Plasmodium falciparum*. The diffusion of pathogenic strains, resistant to traditional antimalarial treatments, urgently requests the development of new therapies. *P. falciparum* belongs to Apicomplexa, a phylum consisting of unicellular, obligate intracellular parasites which possess an organ of algal origin, the apicoplast. This organelle has been shown to be required for pathogen survival becoming a known site of action of antimalarial compounds. In the apicoplast of *P. falciparum* a ferredoxin-$NADP^+$ reductase (PfFNR) has been identified. This enzyme, in conjunction with ferredoxin, is directly involved in the electron transfer from NADPH to LytB which catalyzes the last step of the mevalonate-independent isoprenoid biosynthesis, an essential pathway of the parasite. The crystallographic structure of PfFNR revealed that the enzyme binds the substrate NADP(H) in an unusual way respect to other FNRs and showed that in the NADP(H) binding site are located two basic residues, His286 and Lys249 conserved within the *Plasmodium* genus but not in other plant-type homologues.

Aim of this work has been to clarify the role of His286 and Lys249 in substrate binding and catalysis, and to identify and characterize a first set of PfFNR inhibitors, selected by different approaches. In particular, I have undertaken the characterization of variants of PfFNR obtained by site-directed mutagenesis, in which His286 and Lys249 have been replaced. Moreover I studied *in vitro* a series of enzyme inhibitors selected by virtual screening, exploiting the enzyme tridimensional structure, and by screening of a compounds library.

The features of PfFNR, highligthed by the studies that I performed on the various enzyme forms, make PfFNR an attractive drug target, suitable for the development of novel antimalarial compounds.

2

MATERIALS AND METHODS

2.1 MOLECULAR BIOLOGY

2.1.1 SITE-DIRECTED MUTAGENESIS AND PLASMID CONSTRUCTION

Amino acyl replacements were introduced in the gene encoding wt PfFNR and PfFNR-C99A, using the QuikChange® Lightning Site-Directed Mutagenesis Kit (Stratagene). The procedure was carried out following the manifacturer's instructions, using the plasmid pET-PfFNR as the template for the replacements of His286 and Lys249, and pET-PfFNR-C99A for the replacement of Cys284. The couples of complementary oligonucleotides used are shown in Table 2.1. The plasmids carrying the mutations were named pET-PfFNR-K249A, pETPfFNR-C99A-C284S, pET-PfFNRH286L, pET-PfFNR-H286K, pET-PfFNR-H286Q and pET-PfFNR-H286A, respectively. All these plasmids direct the expression of the respective PfFNR forms with an N-terminal His-tag. The insert of all expression plasmids was fully sequenced to exclude the presence of artifacts.

Table 2.1. Oligonucleotide primers used for the mutagenesis

Underlined nucleotides indicate mismatches sites in the mutagenesis primers.

Primer	*Nucleotide sequence*
Lys249Ala	5'-TATACATTATGTTTTCTCTTAT**GCA**CAAAATTCAGATGCAACAAG-3'
Lys249Ala	5'-CTTGTTGCATCTGAATTTTG**TGC**ATAAGAGAAAACATAATGTATA-3'
Cys284Ser	5'-TAATTATAAATGTGAATTATATATA**A**GTGGTCACAAATCAATAAG-3'
Cys284Ser	5'-CTTATTGATTTGTGACCAC**T**TATATATAATTCACATTTATAATTA-3'
His286Leu	5'-GAATTATATATATGTGGT**CTG**AAATCAATAAGATATAAAGTTATG-3'
His286Leu	5'-CATAACTTTATATCTTATTGATTT**CAG**ACCACATATATATAATTC-3'
His286Lys	5'-GAATTATATATATGTGGT**AAA**AAATCAATAAGATATAAAGTTATG-3'
His286Lys	5'-CATAACTTTATATCTTATTGATTT**TTT**ACCACATATATATAATTC-3'
His286Gln	5'-GAATTATATATATGTGGT**CAG**AAATCAATAAGATATAAAGTTATG3'
His286Gln	5'-CATAACTTTATATCTTATTGATTT**CTG**ACCACATATATATAATTC-3'
His286Ala	5'-GAATTATATATATGTGGT**GCC**AAATCAATAAGATATAAAGTTATG-3'
His286Ala	5'-CATAACTTTATATCTTATTGATTT**GGC**ACCACATATATATAATTC-3'

The ORF encoding the mature form of PfFNR-C99A was excised from pET-PfFNR as a *Nco*I/*Xho*I fragment and inserted in a customized version of vector pET SUMO (Invitrogen) containing unique *Nco*I and *Xho*I restriction sites yielding the plasmid pET-SUMO-PfFNR-C99A (Figure 2.1). The resulting recombinant protein polyHis-SUMO-PfFNR-C99A is a fusion composed by a polyHis-tag, a small ubiquitin-like modifier (SUMO) unit and PfFNR-C99A. After the cleavage with the SUMO-specific Senp2 protease, polyHis-SUMO-PfFNR-C99A is expected to yield a PfFNR-C99A form that includes extra Ser, Met and Gly.

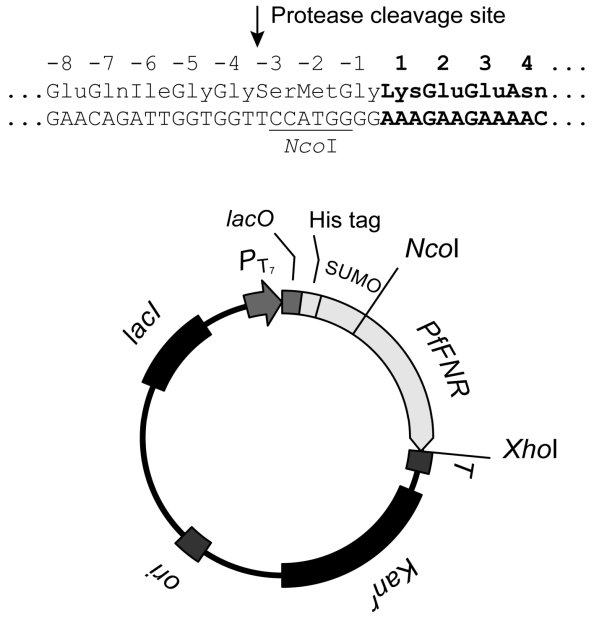

Figure 2.1. Map of pET-SUMO-PfFNR-C99A.

2.2 PROTEIN OVEREXPRESSION AND PURIFICATION

2.2.1 EXPRESSION TEST OF Poly-His-SUMO-PfFNR-C99A

E. coli cells Rosetta (DE3) transformed with the plasmid pETSUMO-PfFNR-C99A were used to inoculate 2xYT medium (500 ml) containing 30 μg/ml kanamycine and grown at 20 °C under orbital shaking (220 rpm). When the A_{600} of the colture reached a value of about 0.8, induction was obtained by addition of isopropyl-thio-β-galactoside (IPTG, 0.1 mM, final concentration). Aliquots of cells were harvested at different times after IPTG addition by centrifugation. To prepare soluble extracts, each aliquot of cells was resuspended in 50 mM NaH_2PO_4, pH 8.0, containing 500 mM NaCl, 5 mM imidazole, 1 mM β-mercaptoethanol and Complete EDTA-free protease inhibitor cocktail (Roche) according to manifacturer's instructions. The cell suspensions were disrupted by sonication with Branson Model 250 Sonifier (6 x 10 s cycles). Each crude extract was obtained by centrifugation at 13000 rpm for 45 min at 4 °C. Aliquots of each crude extract were used for protein and activity assays and SDS-PAGE.

2.2.2 PURIFICATION OF PfFNR-C99A AS CLEAVABLE FUSION WITH SUMO PROTEIN

E. coli cells Rosetta (DE3) harboring the plasmid pETSUMO-PfFNR-C99A were used to inoculate 200 ml of 2xYT medium containing kanamycine at final concentration 30 μg/ml. The colture was grown overnight under orbital shaking (220 rpm) at 37 °C and was used to inoculate 12 l of 2xYT medium at 20 °C containing 30 μg/ml kanamycine in a bioreactor. When the colture reached an optical density at 600 nm between 0.8 and 1, IPTG was added to a final concentration of 0.1 mM. Expression of poly-His-SUMO-PfFNR-C99A was induced for 24 hours. Cells were harvested by centrifugation at 6000 rpm in a Sorvall GSA rotor for 10 min at 4 °C. Tipically, 6 g of wet cell paste was obtained from 1 liter of cells colture. The cell paste was suspended in 2.5 volumes of 50 mM NaH_2PO_4, pH 8.0 containing 500 mM NaCl, 5 mM imidazole, 1 mM β-mercaptoethanol and Complete EDTA-free protease inhibitor cocktail (Roche) according to manifacturer's instruction. Then the cell suspension was disrupted by sonication with Branson Model 250 Sonifier (6 x 1 min cycles). The crude extract was obtained by centrifugation for 60 min at 18000 rpm and 4 °C in a Sorvall SS34 rotor. After centrifugation aliquots of crude extract were used for NADPH-$K_3Fe(CN)_6$ reductase activity, protein assay and SDS-PAGE. The soluble

fraction was loaded on HisTrap™ HP column prepacked with precharged Ni Sepharose™ High Performance (GE Healthcare) and equilibrated in 50 mM NaH_2PO_4, pH 8.0 containing 500 mM NaCl, 5 mM imidazole, 10% glycerol and 1 mM β-mercaptoethanol (Buffer A). The molarity of imidazole in the buffer A was brought to 20 mM and then used for extensive washing. Poly-His-PfFNR-C99A was eluted with 200 mM imidazole in buffer A. After the column, the enzyme has been desalted by gel filtration on Hi Trap™ Desalting column (Amersham Biosciences) equilibrated in 50 mM Tris-HCl, pH 7.4 containing 200 mM NaCl, 10% glycerol and 1 mM DTT.

The hexahistidine affinity tag and SUMO moiety were removed by digestion with Poly-His-senp2 protease using a ratio 1/70 (w/w) between protease and Poly-His-PfFNR-C99A. The digestion mixture was incubated at 20 °C for 30 min. In order to separate the cleaved protein from both protease and the residual uncleaved protein, the digestion mixture was loaded on Ni Sepharose™ High Performance column exploiting the affinity, altough weak, of mature PfFNR-C99A for the resin. For this second purification step the same buffer was used as the previous step on Ni Sepharose™ High Performance (GE Healthcare) column. PfFNR-C99A was eluted with 20 mM imidazole. Then the mature PfFNR-C99A was desalted by gel filtration on Hi Trap™ Desalting column (Amersham Biosciences) equilibrated in 50 mM Tris-HCl, pH 7.4 containing 10% glycerol and 1 mM DTT.

2.2.3 PURIFICATION OF PfFNR FORMS

For the overproduction of PfFNR-H286K, PfFNR-H286L, PfFNR-H286Q, PfFNR-H286A, PfFNR-K249A and PfFNR-C99A-C284S, *E. coli* Rosetta (DE3) cells harboring the plasmids pET-PfFNR-H286L, pET-PfFNR-H286K, pET-PfFNR-H286Q and pET-PfFNR-H286A, pET-PfFNR-K249A, pETPfFNR-C99A-C284S, respectively, were used to inoculate 200 ml of 2xYT medium containing kanamycine at final concentration 30 μg/ml. The colture was grown overnight under orbital shaking (220 rpm) at 37 °C and was used to inoculate 5 x 0.5 l of the same liquid colture medium at 20 C°, 220 rpm. When the colture reached an optical density at 600 nm between 0.8 and 1, IPTG was added to a final concentration of 0.1 mM. Expression of the PfFNR forms was induced for 24 hours. Cells were harvested by centrifugation at 6000 rpm in a Sorvall GSA rotor for 10 min at 4 °C. Tipically, 15 g of wet cell paste was obtained from 2.5 l of cells colture. The cell paste was suspended in 2.5 volumes of 50 mM NaH_2PO_4, pH 8.0, 500 mM NaCl, 5 mM imidazole, 1

mM PMSF and 1 mM β-mercaptoethanol, and was disrupted by sonication with Branson Model 250 Sonifier (6 x 1 min cycles). The crude extract was obtained by centrifugation for 60 min at 18000 rpm and 4 °C in a Sorvall SS34 rotor. After centrifugation aliquots of crude extract were used for NADPH-$K_3Fe(CN)_6$ reductase activity, protein assay and SDS-PAGE. The clarified cell-free extract was loaded on a Ni Sepharose™ High Performance column (GE Healthcare) pre-equilibrated in 50 mM NaH_2PO_4, pH 8.0 containing 500 mM NaCl, 5 mM imidazole, 10% glycerol and 1 mM β-mercaptoethanol (Buffer A). Extensive washing was performed with buffer A containing 20 mM imidazole. The enzyme was eluted with a 20-500 mM imidazole gradient under the conditions recommended by the resin manufacturer. The best fractions were pooled together, 5 mM EDTA was added, and ammonium sulfate was added to 15% saturation, for chromatography on a Phenyl-Sepharose High Performance column (GE Healthcare). Ammonium sulfate in a decreasing gradient of saturation from 15% to 0% in buffer B (50 mM Tris-HCl, pH 7.4, containing 10% glycerol and 1 mM DTT) was used to elute the enzyme. The best fractions were pooled and precipitated at 70% ammonium sulfate saturation. The enzyme was solubilized in buffer B and desalted on a Hi Trap™ Desalting column (Amersham Biosciences). After incubation for 48 hours at 16 °C with 1/500 (w/w) Factor Xa (Pierce) to cleave off the His-tag, the mixture was loaded again on a Ni Sepharose™ High Performance column (GE Healthcare). Owing to the moderate intrinsic affinity of PfFNR forms to the nickel ion, the enzyme was retained by the column even in the absence if the His-tag, and was specifically eluted with 20 mM imidazole. The FNR-containing fractions were concentrated by ultrafiltration, desalted by gel filtration on a Hi Trap™ Desalting column (Amersham Biosciences), and stored at -80 °C in 50 mM Tris-HCl , pH 7.4 containing 10% glycerol and 1 mM DTT.

2.3 PROTEIN ASSAYS

Protein concentration of crude extract was determined with the Biuret method (Thieler H. *et al.*, 1966) and that of all the other sample by the Bradford method (Bradford M., 1976), with bovine serum albumine (BSA) as the reference protein, using Amresco Bradford Reagent.

2.4 SDS-PAGE

SDS-PAGE was carried out on 8x10 cm, 1.5 mm thick gels in a Hoefer SE260 apparatus using the Laemmli method (Laemmli U. K., 1960). Total acrylamide/bis-acrylamide concentration in running gels was 12%. Gels were stained with Comassie Blue and destained by diffusion in 30% ethanol and 10% acetic acid.

2.5 WESTERN BLOT

For Western analysis, soluble extract and proteins fractionated by SDS-PAGE were transferred to Hybond-C extra membrane (Amersham Pharmacia Biotech) using blotting apparatus (BioRad). The blot was incubated with the anti-PfFNR polyclonal serum, and immunodetection was performed using Anti-rabbit IgG alkaline phosphatase conjugated.

2.6 N-TERMINAL SEQUENCE ANALYSIS

For N-terminal sequence analysis determination both the mature and the truncated PfFNR-C99A were electroblotted on a PVDF membrane and analyzed by a pulsed-liquid sequencer equipped with a PHT analyser (Procise model 491, Applied Biosystems) in the Prof. Gabriella Tedeschi laboratory (Dipartimento di Patologia Animale, Igiene e Sanità Pubblica Veterinaria, Università degli Studi di Milano, Milan, Italy).

2.7 ACTIVITY ASSAYS

2.7.1 STEADY-STATE KINETICS

2.7.1.1 STANDARD ACTIVITY

Standard diaphorase activity was measured in 1 ml of reaction mixture containing:

2 μg/ml	Glucose-6-phosphate dehydrogenase
0.1 mM	$NADP^+$
2.5 mM	Glucose-6-phosphate
100 mM	Tris-HCl pH 8.2
1 mM	$K_3Fe(CN)_6$

After the addition of ~ 25 nM PfFNR forms, reaction was monitored spectrophotometrically by following ferricyanide reduction at 420 nm (ε_{420} = 1.025 $mM^{-1}cm^{-1}$). The standard activity is expressed in U/mg (μmol of product/min/mg of enzyme) or in U/FAD (μmol of product/min/μmol of enzyme) and it has been measured after each chromatographic step.

Standard activity using DCPIP as artificial electron acceptor was determined in 1 ml reaction mixture containing:

2 μg/ml	Glucose-6-phosphate dehydrogenase
0.1 mM	$NADP^+$
2.5 mM	Glucose-6-phosphate
100 mM	Tris-HCl pH 8.2
30 μM	DCPIP

After the addition of ~ 7.5 nM PfFNR, reaction was monitored spectrophotometrically by following DCPIP reduction at 600 nm (ε_{600} = 21.4 $mM^{-1}cm^{-1}$).

Standard activity using cytochrome *c* as electron acceptor was determined in 1 ml reaction mixture containing:

0.1 mM	NADPH
43 µM	cytochrome *c*
100 mM	Tris-HCl pH 8.2

After the addition of ~ 15 nM PfFNR forms, reaction was monitored spectrophotometrically by following cytochrome *c* reduction at 550 nm (ε_{550}= 19.5 $mM^{-1}cm^{-1}$). The following reaction mechanism has been considered:

$$NADPH + I_{ox} \leftrightarrow NADP^+ + I_{red} + H^+$$

$$I_{red} + O_2 \rightarrow I_{ox} + O_2^-$$

$$O_2^- + cyt\ c_{ox} \rightarrow O_2 + cyt\ c_{red}$$

where *I* = I24 or I27

Standard activity using *p*-iodonitritetrazolium (INT) as electron acceptor was determined in 1 ml reaction mixture containing:

0.1 mM	NADPH
50 mM	NaCl
100 mM	MOPS-NaOH pH 7 or 100 mM Tris-HCl pH 8.2
0.1 mM	INT
60 µM	compound of Prestwick Chemical Library®

After the addition of ~ 10 nM PfFNR, reaction was monitored by following the appearance of a pink coloration indicating the progress of the reaction.

2.7.1.2 DETERMINATION OF KINETIC PARAMETERS

Steady-state kinetic parameters for NAD(P)H-$K_3Fe(CN)_6$ reductase reaction and NADPH-DCPIP reductase reaction were determined by varying independently the concentration of both NAD(P)H and the electron acceptor. The NADH- $K_3Fe(CN)_6$ reductase activity of the PfFNR-K249A form was measured omitting the NADPH-regenerating system. Initial velocity data were fitted to the equation for a competitive inhibition (1) in the case of ferricyanide and for a ping-pong bi-bi (2) in the case of DCPIP. The inhibitory effect of 2'-P-AMP on the NADPH-DCPIP reductase reaction catalyzed by the PfFNR forms was studied by independently varying the concentration of NADPH and that of the inhibitor at a fixed concentration of DCPIP (20 μM). Initial velocity data were then fitted to the equation for a competitive inhibition (1).

$$v = \frac{V_{max}[NADPH]}{K_m\left(1+\frac{[I]}{K_i}\right)+[NADPH]} \quad (1)$$

K_i = competitive inhibition constant

I = inhibitor

$$v = \frac{V_{max}\,[A][B]}{(K_B[A]+ K_A[B]+ [A][B])} \quad (2)$$

A = NADPH

B = electron acceptor (DCPIP)

K_A, K_B = Michaelis constants

Steady-state kinetic parameters for NADPH-$K_3Fe(CN)_6$ reductase reaction at different pH were determined as described above. From pH 6.25 to 8 the activity was assayed in 50 mM sodium phosphate and from pH 8.5 to 10.25 it was assayed in 50 mM sodium carbonate.

2.7.1.3 DETERMINATION OF IC_{50} OF INHIBITORS

Both NADPH-$K_3Fe(CN)_6$ reductase reaction and NADPH-DCPIP reductase reaction were used to determine IC_{50} values omitting the NADPH-regenerating system. The reaction mixture contained:

100 mM	Tris-HCl pH 8.2
0.1 mM	NADPH

Moreover it has been added to the mixture increasing concentrations of inhibitor and 1 mM $K_3Fe(CN)_6$, in the case of NADPH-$K_3Fe(CN)_6$ reductase reaction, and 30 μM DCPIP, in the case of NADPH-DCPIP reductase reaction. The initial velocity data were reported as percentage of residual activity and were fitted to the equation for determination of parameter IC_{50} (3):

$$y = \frac{100\%}{1+\left(\frac{x}{IC_{50}}\right)^{s}} \qquad (3)$$

x = % residual activity

s = slope factor

2.7.1.4 DETERMINATION OF INHIBITION CONSTANT OF COMPOUNDS SELECTED BY VIRTUAL SCREENING

Inhibition constants values (K_i) were determined for the NADPH-$K_3Fe(CN)_6$ reductase reaction and NADPH-DCPIP reductase reaction as described in paragraph 3.7.1.2. The electron acceptor concentration has been kept constant, 30 μM DCPIP and 100 μM $K_3Fe(CN)_6$ respectively. In order to evoid that ferricyanide inhibitor effect interferes with that of the compounds analyzed, $K_3Fe(CN)_6$ concentration was lower in comparison with standard acitivity assays. Initial velocity data were then fitted to the equation for a mixed inhibition (4) describing an inhibitory effect which affects both the apparent k_{cat}/K_m and k_{cat} of the enzyme. This analysis provides two inhibition constants K_i and K_i'.

$$v = \frac{V_{max}\,[NADPH]}{K_m\left(1+\frac{[I]}{K_i}\right)+\left(1+\frac{[I]}{K_i'}\right)[NADPH]} \qquad (4)$$

K_i = competitive inhibition constant

K_i' = uncompetitive inhibition constant

I = inhibitor

2.8 INHIBITION STUDIES WITH EBSELEN

2.8.1 SPECTROPHOTOMETRIC ANALYSIS

2.8.1.1 KINETIC OF EBSELN INHIBITION OF PfFNR

Standard diaphorase activity with ferricyanide was measured for PfFNR-C99A, PfFNR-C99A-C284S, SoFNR, SoFNR-C272S and FprA as described in paragraph 3.7.1.1 in presence of different concentrations of ebselen. The same reactions were carried out in 50 mM HEPES-NaOH pH 7.0. Each time course was fitted with curves describing the slow onset of complete enzyme inactivation during the assay, according to a single exponential decay (5).

$$A = A_0 - v_s t - \frac{(v_i - v_s)(1 - e^{-\mathrm{kt}})}{k} \qquad (5)$$

A = absorbance at time t

A_0 = initial absorbance

v_i = initial velocity of the catalyzed reaction

v_s = steady-state (final) velocity of the catalyzed reaction

k = apparent kinetic constant of EI formation

t = reaction time

Apparent kinetic constant (k) values in function of ebselen concentrations were consistent with a simple bimolecular mechanism. The second order inhibition rate constant (k_{ebselen}) were calculated by using equation (6):

$$k = k_{\mathrm{ebselen}}\,[\mathrm{ebselen}] \qquad (6)$$

2.8.1.2 CHARACTERIZATION OF EBSELEN IRREVERSIBLE INHIBITION

PfFNR-C99A (2 μM) and wt PfFNR (2 μM) were incubated in 50 mM TrisHCl pH 7.4, 10% glycerol with 10 μM ebselen at 25 °C. Aliquots of the incubation mixture were withdrawn periodically and diluted in the standard NADPH-$K_3Fe(CN)_6$ reductase assay mixture (see paragraph 3.7.1.1).

2.8.1.3 EFFECT OF REDUCED GLUTATHIONE ON EBSELEN INHIBITION

PfFNR-C99A (2 μM) was incubated in 50 mM TrisHCl pH 7.4, 10% glycerol with 0.1 mM GSH at 25 °C either with or without ebselen. Aliquots of the incubation mixture were withdrawn periodically and diluted in the standard NADPH-$K_3Fe(CN)_6$ reductase assay mixture (see paragraph 3.7.1.1).

2.8.1.4 EFFECT OF NADPH ON EBSELEN INHIBITION

Standard diaphorase activity with ferricyanide was measured for PfFNR-C99A as described in paragraph 3.7.1.1 in presence of different concentrations of NADPH, keeping constant ebselen concentration (10 μM). Each time course was fitted with equation (5).

2.8.1.5 EFFECT OF EBSELEN TARGETING THE Cys RESIDUES

wt PfFNR (2 μM), PfFNR-C99A (2 μM) and PfFNR-C99A-C284S (25 μM) were incubated in 50 mM HEPES-NaOH, pH 7.0 with different concentrations of ebselen yielding an inhibitor/enzyme molar ratio between 0.5/1 and 10/1. Aliquots of the incubation mixture were withdrawn periodically and diluted in the standard NADPH-$K_3Fe(CN)_6$ reductase assay mixture (see paragraph 3.7.1.1) untill no variation of residual activity was observed.

2.8.2 SPECTROFLUORIMETRIC ANALYSIS

Studies about FAD release from PfFNR forms promoted by ebselen were performed spectrofluorimetrically at 25 °C using spectrofluorimeter Cary Eclipse (Varian). PfFNR-C99A (1 μM) and PfFNR-C99A-C284S (1 μM) were incubated either in 100 mM HEPES-NaOH, pH 7.0 or 100 mM TrisHCl, pH 8.2 in presence of different ebselen concentrations. Flavin fluorescence was measured as emission wavelength at 530 nm after an excitation at 450 nm.

2.9 NADP$^+$ TITRATION OF PfFNR FORMS

Titration of oxidized PfFNR forms with NADP$^+$ were performed spectrophotometrically at 15 °C. The enzyme was diluted to a final concentration of about 20 μM in 50 mM Tris-HCl, pH 7.6 using a Cary 100 (Varian) double-beam spectrophotometer. Difference spectra were computed by subtracting from each spectrum that obtained in absence of ligand, after correction for dilution. K_d values were obtained by fitting data sets by non-linear regression to the theoretical equation (7) for a 1:1 binding, using the GraFit 4.0 software (Erythacus Software Ltd, Staines, UK). ΔA is the value of the difference spectrum at a selected wavelength; Δε is the difference extinction coefficient at that wavelength of the protein-ligand complex.

$$\Delta A = \Delta\varepsilon \frac{[L]_T + [P]_T + K_d - \sqrt{([L]_T + [P]_T + K_d)^2 - 4[L]_T[P]_T}}{2} \quad (7)$$

$$[L]_T = \frac{V_a}{V_i + V_a}[L]_a$$

$$[P]_T = \frac{V_i}{V_i + V_a}[P]_i$$

$[L]_a$ = concentration of ligand stock solution

V_a = volume of ligand added

$[P]_i$ = protein initial concentration

V_i = initial volume of reaction mixture

2.10 PHOTOREDUCTION EXPERIMENTS

Anaerobic stepwise photoreduction of the FAD prosthetic group of PfFNR forms was performed by the light/EDTA system. In particular the PfFNR forms reduction was achieved by one-electron donation from 5-carba-5-deazariboflavin semiquinone produced by light irradiation, to EDTA serving as the final electron source. Photoreductions were performed in presence of $NADP^+$ and the reactions were carried out at 15 °C in an anaerobic cuvette on ~15 μM PfFNR samples in 50 mM HEPES-NaOH, pH 7.0 containing 10% glycerol, 13 mM EDTA and 1.3 μM 5-carba-5-deazariboflavin. $NADP^+$ was at a 1.2 molar ratio with respect to the enzyme. Reaction solutions were made anaerobic by successive evacuation and flushing with O_2-free N_2. Each mutant was subject to successive short times of illumination to finally reach full reduction of enzyme flavin. Absorption spectra were recorded before and after successive periods of irradiation.

2.11 RAPID KINETICS

Wild-type or mutant PfFNRs (17-20 μM) were reacted with NADPH (0.025-2 mM) at 25 °C in 50 mM HEPES-NaOH, pH 7.0 under anaerobic conditions, using an SF-61 DX2 diode-array stopped-flow spectrophotometer (Hi-Tech Scientific, Bradford-upon-Avon, UK). Briefly, anaerobiosis in the instrument syringes and plumbing was achieved by flushing them with anaerobic 5 mM sodium dithionite in 50 mM Tris-HCl, pH 8.5, which was allowed to scavenge oxygen overnight. Two hours prior to the beginning of the experiment, the dithionite solution was substituted with anaerobic buffer. Prior to stopped-flow studies, enzymes were gel filtered in PD-10 column in 50 mM HEPES-NaOH, pH 7.0 and were made anaerobic in a tonometer by repeated cycles of evacuation and flushing with O_2-free N_2. Substrate solutions were instead made anaerobic by bubbling nitrogen through them for at least 15 min. The rate of flavin reduction was measured by monitoring the decrease in absorbance at 454 nm that results from the decreasing of oxidized flavin upon mixing the enzyme with the substrate. A set of 300 spectra within the 300-700 nm wavelength range was recorded from each shot over total reaction times ranging from 0.5 to 7 s. Absorbance traces at different wavelengths were fitted to exponential decay equations using KinetAsyst version 3.0 (Hi-Tech Scientific).

2.12 CRYSTALLIZATION OF PfFNR-H286K AND PfFNR-H286L

In collaboration with Dr. Mario Milani, Università degli Studi di Milano, recombinant PfFNR-H286K and PfFNR-H286L were crystallized in batch setup under a 1:1 mixture of paraffin and silicon oils, using an Oryx 8 robot (Douglas instruments). PfFNR-H286K was 25 mg/ml in 50 mM Tris-HCl, pH 7.4, containing 1 mM DTT, 2 mM 2'-P-AMP. The well solutions consisted of 20% 2-propanol, 20% PEG 4000 and 0.1 M citrate-NaOH, pH 5.4. Crystal grew under these conditions in ~ 2 weeks.

PfFNR-H286L was crystallized both in its free form and in complex with 2'-P-AMP. Crystals of PfFNR-H286L were obtained by mixing 35 mg/ml PfFNR-H286L in 50 mM Tris-HCl, pH 7.4, containing 1 mM DTT with 1.6 M citrate-NaOH, pH 6.5, while crystals of the PfFNR-H286L-2'-P-AMP complex were obtained by soaking a crystal (grown in 12% PEG 6000, 5% glycerol, 0.1 M cacodylate-NaOH pH 6.5) in a stabilizing solution (18% PEG 6000, 5% glycerol, 0.1 M cacodylate-NaOH pH 6.5 and 3 mM 2'-P-AMP) containing the ligand. Both the crystal forms grew in ~ 3 weeks.

All the crystals were soaked in a cryoprotectant solution obtained by adding up to 25% glycerol to the respective precipitating solution and flash-cooled in liquid nitrogen. X-ray diffraction data were collected at the ID23-1 beamline of ESRF (Grenoble) and at Elettra, Trieste, XRD1.

3

RESULTS

3.1 INHIBITION STUDIES AND CHARACTERIZATION OF COMPOUNDS ACTIVE AGAINST PfFNR

3.1.1 STRUCTURE-BASED VIRTUAL SCREENING

In collaboration with Dr. Mario Milani and Prof. Martino Bolognesi (Università degli Studi di Milano), an *in silico* screening of two virtual libraries of compounds was performed, in order to identify novel molecules inhibiting PfFNR. The program AutoDock (Goodsell, D.S. *et al*., 1996) was used to study the interaction of small, flexible ligands to the known structure of PfFNR. AutoDock was run on two virtual libraries, LOPAC and Diversity Set. The ~1900 compounds of Diversity Set have been isolated by the Developmental Therapeutics Program of the National Cancer Institute whereas LOPAC is obtained from Sigma-Aldrich and it contains ~1300 drug-like compounds, pharmacologically active and commercially available with an high grade purity.

Since the crystal structure of PfFNR was obtained in complex with 2'-P-AMP, the binding site of the substrate analogue was chosen as the target for the screening. Autodock calculates the interaction energy considering deformation energy of the ligand, loss of conformational entropy and desolvatation energy.

With this approach, 34 compounds were identified with binding energy for PfFNR similar or better than that of 2'-P-AMP.

I have experimentally characterized 16 out of these 34 compounds in order to evaluate their actual action on the catalytic properties of PfFNR.

3.1.1.1 DETERMINATION OF IC_{50}

The IC_{50} is the concentration of inhibitor that provides 50% inhibition of the target enzyme. I evaluated this parameter measuring PfFNR catalytic activity using two different artificial substrate as electron acceptors: potassium ferricyanide ($K_3Fe(CN)_6$) and dichlorophenolindophenol (DCPIP) a one-electron and two-electron acceptor, respectively.

3.1.1.1.1 INHIBITION OF NADPH- $K_3Fe(CN)_6$ REDUCTASE REACTION

I found that four compounds, I19, I21, I23 and I27, were able to efficiently inhibit PfFNR with an IC_{50} equal or less than 10 μM, as shown in Table 3.1.
In some cases it was not possible to obtain an IC_{50} value: compound I29 displayed an IC_{50} value too high to be determined, while compound I23, because of its high absorbance at 420 nm, made difficult to monitor the reduction of $K_3Fe(CN)_6$ preventing a reliable measure of residual enzymatic activity. Finally, compound I32 was found to interfere with the enzyme assay, because it turned out to be a good catalyst itself of the reduction of $K_3Fe(CN)_6$ by NADPH.

Inhibitor	IC_{50} $^{K_3Fe(CN)_6}$ (μM)	Inhibitor	IC_{50} $^{K_3Fe(CN)_6}$ (μM)
I8	47.1 ± 2.6	**I27**	9.6 ± 0.5
I19	10.8 ± 0.9	**I28**	115 ± 6
I21	0.170 ± 0.007	**I29**	/ [a]
I22	299 ± 14	**I30**	2116 ± 817
I23	/ [b]	**I31**	221 ± 41
I24	2.05 ± 0.04	**I32**	/ [b]
I25	53.2 ± 3.1	**I33**	226 ± 38
I26	84.9 ± 1.3	**I34**	193 ± 6

[a]: not determined because of the high inhibition constrant of the compound
[b]: not determined because the compound interfere with the measurement of reaction rate

Table 3.1. IC_{50} for NADPH-$K_3Fe(CN)_6$ reductase reaction catalized by PfFNR.

3.1.1.1.2 INHIBITION OF NADPH- DCPIP REDUCTASE REACTION

In order to confirm the results described in the previous paragraph, I measured the IC_{50} for the NADPH-DCPIP reductase reaction. As shown in the Table 3.2, the activity with DCPIP is more sensitive to inhibition than the activity with $K_3Fe(CN)_6$. In particular I19, I21, I24 and I27 have an IC_{50} lower than 2 μM, while I29 was confirmed to be a very poor inhibitor of PfFNR. The study of NADPH-DCPIP reductase reaction allowed to determine the IC_{50} for I23 and I32, even if these value were rather high.

Table 3.2. IC_{50} for NADPH-DCPIP reductase reaction catalized by PfFNR.

Inhibitor	IC_{50}^{DCPIP} (μM)	Inhibitor	IC_{50}^{DCPIP} (μM)
I8	10.3 ± 0.2	**I27**	0.78 ± 0.03
I19	1.8 ± 0.7	**I28**	25.6 ± 0.5
I21	0.076 ± 0.003	**I29**	-
I22	160 ± 6	**I30**	257 ± 11
I23	36 ± 1	**I31**	97.8 ± 5.3
I24	0.75 ± 0.02	**I32**	755 ± 51
I25	20.7 ± 0.7	**I33**	76.7 ± 2.9
I26	25.6 ± 0.5	**I34**	380 ± 129

3.1.1.2 SELECTIVITY OF INHIBITORS

In vitro characterization of compounds selected by virtual screening allowed to identify five molecules, *i.e.* I8, I19, I21, I24 and I27, as good inhibitors of PfFNR. I evaluated their selectivity by measuring IC_{50} on homologue FNR of *Toxoplasma gondii* (TgFNR) and maize root (rFNR). I21 has been excluded from this analysis because this compound is known to be active against a variety of NAD(P)(H)-dependent oxidoreductases (Thompson D. C. *et al.*, 1995).

3.1.1.2.1 INHIBITION OF NADPH- $K_3Fe(CN)_6$ REDUCTASE REACTION OF TgFNR AND rFNR

As shown in Table 3.3, I19 and I8 resulted to be highly specific for Apicomplexa FNRs. In particular, I8 is completely inactive against rFNR, while I24 and I27 are able to inhibit all FNRs tested.

Table 3.3. IC_{50} of PfFNR inhibitors for NADPH- $K_3Fe(CN)_6$ reductase reaction measured for homologous FNRs.

	IC_{50} $K_3Fe(CN)_6$ (μM)		
	PfFNR	**TgFNR**	**rootFNR**
I8	47.1 ± 2.6	52 ± 1	-
I19	10.8 ± 0.9	13.1 ± 0.8	221 ± 78
I24	2.05 ± 0.04	0.59 ± 0.02	8.6 ± 0.4
I27	9.6 ± 0.5	6.1 ± 0.4	12.6 ± 0.3

3.1.1.2.2 INHIBITION OF NADPH-DCPIP REDUCTASE REACTION OF TgFNR AND rFNR

The effect of the inhibitors on NADPH-DCPIP reductase activity is similar to that observed with $K_3Fe(CN)_6$ as electron acceptor. Table 3.4 points out that I8 and I19 are good inhibitors of TgFNR but are poorly active against FNR from plant roots. Moreover I24 and I27 are selective for Apicomplexa FNRs also in case of DCPIP reductase activity.

Table 3.4. IC_{50} of PfFNR inhibitors for NADPH- DCPIP reductase reaction measured for homologous FNRs.

	IC_{50}^{DCPIP} (µM)		
	PfFNR	**TgFNR**	**rFNR**
I8	10.3 ± 0.2	7.6 ± 0.7	127.6 ± 5.7
I19	1.8 ± 0.7	1.4 ± 0.2	190.9 ± 16.7
I24	0.75 ± 0.02	0.47 ± 0.07	-
I27	0.78 ± 0.03	0.62 ± 0.03	3.68 ± 0.06

3.1.1.3 DETERMINATION OF INHIBITION CONSTANTS

To further characterize the five best PfFNR inhibitors and to elucidate their mechanism of action, activity assays were performed by varying the concentration of both NADPH and inhibitor, using a mixed-inhibition model to fit the initial rate data.

In Table 3.5 and 3.6 are reported kinetic parameters of PfFNR for both the diaphorase activities. Mixed inhibition is described by two inhibition constants (K_i and K'_i). K_i (competitive inhibition constant) measures the effect of inhibitor on the apparent k_{cat}/K_m of the enzyme, while K'_i (uncompetitive inhibition constant) measures the effect of inhibitor on the apparent k_{cat}. For all the inhibitors considered, the inhibition mechanism showed that both the inhibition constants are statistically significant, making impossible to simplify the inhibition mechanism. Moreover, in each case, the two constants resulted to be significantly different among them, with K_i lower than K'_i, thus excluding a pure non-competitive inhibition pattern.

In summary, all the compounds considered displayed a mixed-type inhibition mechanism, with a predominant competitive component with respect to NADPH.

Table 3.5. Inhibition kinetic parameters for the NADPH-$K_3Fe(CN)_6$ reductase reaction

NADPH-$K_3Fe(CN)_6$ reductase reaction					
	k_{cat} (e^- eq s^{-1})	K_m^{NADPH} (μM)	K_i (μM)	K'_i (μM)	k_{cat} / K_m^{NADPH} (e^- eq s^{-1} μM^{-1})
I8	162.1 ± 4.4	39.8 ± 6.7	12.8 ± 3.7	99.8 ± 21.5	4.1 ± 0.7
I19	159.9 ± 4.7	42.6 ± 7.1	3.6 ± 1.3	8.5 ± 1.1	4.02 ± 0.69
I21	175.5 ± 6.8	41.1 ± 8.4	0.19 ± 0.09	0.42 ± 0.08	4.3 ± 0.9
I24	189.9 ± 4.6	41.3 ± 5.2	0.33 ± 0.06	3.2 ± 0.5	4.6 ± 0.6
I27	134.2 ± 3.1	31.6 ± 4.3	4 ± 1	11.1 ± 1.1	4.2 ± 0.6

Table 3.6. Inhibition kinetic parameters for the NADPH-DCPIP reductase reaction

NADPH-DCPIP reductase reaction					
	k_{cat} (e^- eq s^{-1})	K_m^{NADPH} (μM)	K_i (μM)	K'_i (μM)	k_{cat} / K_m^{NADPH} (e^- eq s^{-1} μM^{-1})
I8	68.7 ± 1.7	43 ± 6	16.3 ± 5.5	51.4 ± 9.2	1.6 ± 0.2
I19	70.9 ± 1.6	42.5 ± 5.7	4.1 ± 1.1	13.9 ± 1.8	1.7 ± 0.2
I21	27.4 ± 0.7	39.6 ± 5.5	0.028 ± 0.008	0.09 ± 0.01	0.7 ± 0.1
I24	56.3 ± 1.3	29 ± 4	0.21 ± 0.05	1.2 ± 0.2	1.9 ± 0.3
I27	68.22 ± 2.04	39.6 ± 6.5	1.4 ± 0.5	5.7 ± 1.1	1.7 ± 0.3

3.1.1.4 EFFECT OF QUINONIC INHIBITORS ON NADPH-CYTOCHROME *c* REDUCTASE REACTION OF PfFNR

Reduced quinons are reactive towards molecular oxygen, being re-oxidated by it with generation of ROS. Cytochrome *c* (Cyt *c*) is sensitive to superoxide ion, in particular Cyt *c* is reduced by superoxide with an easily detectable raise of extinction coefficient at 550 nm. Moreover, in absence of the physiological substrate ferredoxin, FNRs possesses only a very weak NADPH-Cyt *c* reductase activity. For these reasons I considered the effect of quinonic inhibitors on this activity a good critirion to evaluate their capability to act as substrate of PfFNR. Figure 3.1A and 3.1B show the increase of Cyt *c* reductase activity of PfFNR as a function of I24 and I27 concentration. Altogether this results suggests that both I24 and I27 are probably reduced by PfFNR in presence of NADPH and rapidly reoxidized by O_2, generating the superoxide anion.

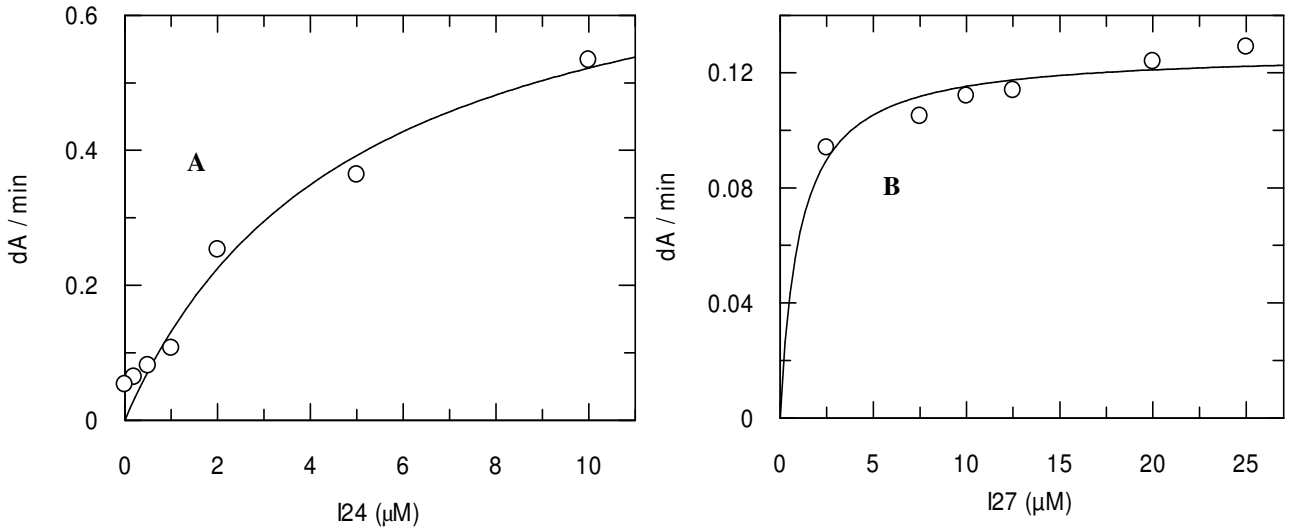

Figure 3.1A and 3.1B. Effect of quinonic compounds I24 and I27 on NADPH-cyt *c* reductase reaction catalyzed by PfFNR.

3.1.2 PfFNR INHIBITION BY EBSELEN

In order to identify inhibitors of PfFNR, I screened a library of compounds called Prestwick Chemical Library®, kindly provided by Prof. Pierfausto Seneci (Università degli Studi di Milano). The library contains 1200 small drug-like molecules, all commercially available. These compounds have been selected for their high chemical and pharmacological diversity as well as for their known bioavailability and safety in humans.
I perform the screening by monitoring the NADPH-INT reductase activity of PfFNR because the reduction of INT gives an easily observable formation of a colored product. Using this activity assay, I identified ebselen ((2-phenyl-1,2-benzisoselenazol-3(2H)-one) as a powerful inhibitor of PfFNR activity. This compound is an anti-inflammatory seleno-organic compound that has been extensively studied in the past. The particular interest in this molecule is due to its enzyme-like catalytic activity. In particular ebselen mimics glutathione peroxidase (GPx) activity by reducing a hydroperoxide at the expense of thiol group of a molecule like glutatione (Muller *et al.*, 1984).
Moreover ebselen reacts with thiol groups of proteins by forming a selenylsulphide bond and it has been reported to inhibit at low concentrations a variety of enzymes such as lipoxygenase, nitric oxide syntase, protein kinase C, NADPH-cytocrome P-450 reductase and NADPH oxidase (Schewe, 1995). Most of the enzymes inhibited by ebselen are involved in inflammatory and oxidative processes so it is reasonable to assume that the inibitory effect observed *in vitro* may contribute to the anti-inflammatory and anti-oxidant action of ebselen *in vivo.* Indeed, it has been demonstrated that ebselen is able to reduce oxidative stress arised after a cardiac ischemia (Maulik *et al.*, 1998).
Ebselen is a promising drug because of some characteristics such as low toxicity, high stability and also beacuse its selenium moiety is not liberated during biotrasformation and therefore it does not interfere with selenium metabolism of the organism.
Several years ago it has been shown that ebselen possesses an antimalarial activity *in vitro* against chloroquine-resistant and chloroquine-sensitive *P. falciparum* strains in the asexual stages. Ebselen is able to block each stages of *P. falciparum* life cycle. Additionally this compound has no cytostatic or cytotoxic effects on human epatocytes indicating a selective inhibition of *plasmodium* (Hüter *et al.*, 1989).

3.1.2.1 CHARACTERIZATION OF EBSELEN IRREVERSIBLE INHIBITION

In order to evaluate the reversibility of ebselen action on the enzyme, PfFNR was incubated with ebselen and the residual catalytic activity at different incubation times was assayed after a dilution of 200-fold. Plots of residual activity versus time showed that the activity decayed untill a complete inhibition ensued after 10 min reaction (Figure 3.3). Moreover, ebselen removal by dilution did not result in any recovery of activity indicating an irreversible mechanism of inhibition. Same results were obtained measuring residual activity of the enzymatic variant PfFNR-C99A indicating that ebselen action does not involve enzyme dimerization (Figure 3.2). The addition of DTT or β-mercaptoethanol to the enzyme-inhibitor incubation mixture did not restore the catalytic activity strongly supporting the hypotesis of a non-reversible mechanism.

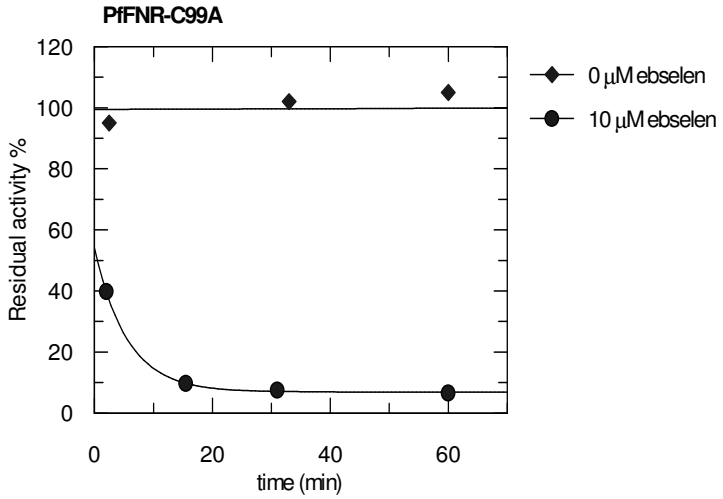

Figure 3.2. Residual activity of PfFNR-C99A evaluated after ebselen dilution

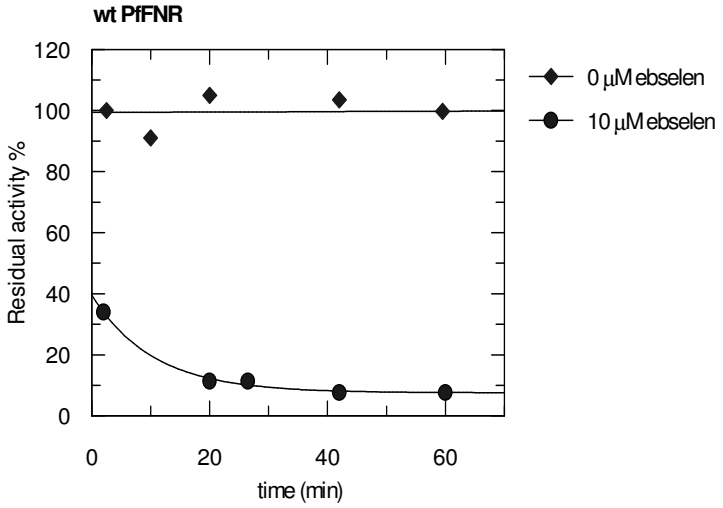

Figure 3.3. Residual activity of wt PfFNR evaluated after ebselen dilution

3.1.2.2 EFFECT OF REDUCED GLUTATHIONE ON PfFNR INACTIVATION BY EBSELEN

Glutathione is a tripeptide containing glycine, cysteine and glutamate. The reduced form (GSH) is a strong intracellular antioxidant. In particular glutathione reduces disulfide bond between cytoplasmic proteins acting as electron donor. Moreover it reacts with peroxides (ROOH), generated by oxidative stress, converting them into alcohol and water (ROH + H_2O). This reaction is catalyzed by glutathione peroxidase and it has been demonstrated that ebselen is able to mimic peroxidase activity reacting with GSH.

In order to verify the hypotesis that ebselen could act on sulphydryl groups of PfFNR, I studied the capability of GSH to prevent the inactivation of the enzyme.

PfFNR-C99A has been incubated with respectively 20, 40 and 60 μM of ebselen, either in the absence or in the presence of 100 μM GSH. As shown in the plots (Figure 3.4), GSH is able to protect PfFNR from inactivation suggesting indirectly that ebselen inhibits PfFNR acting on one or more cysteine residues which are important for enzyme activity or stability.

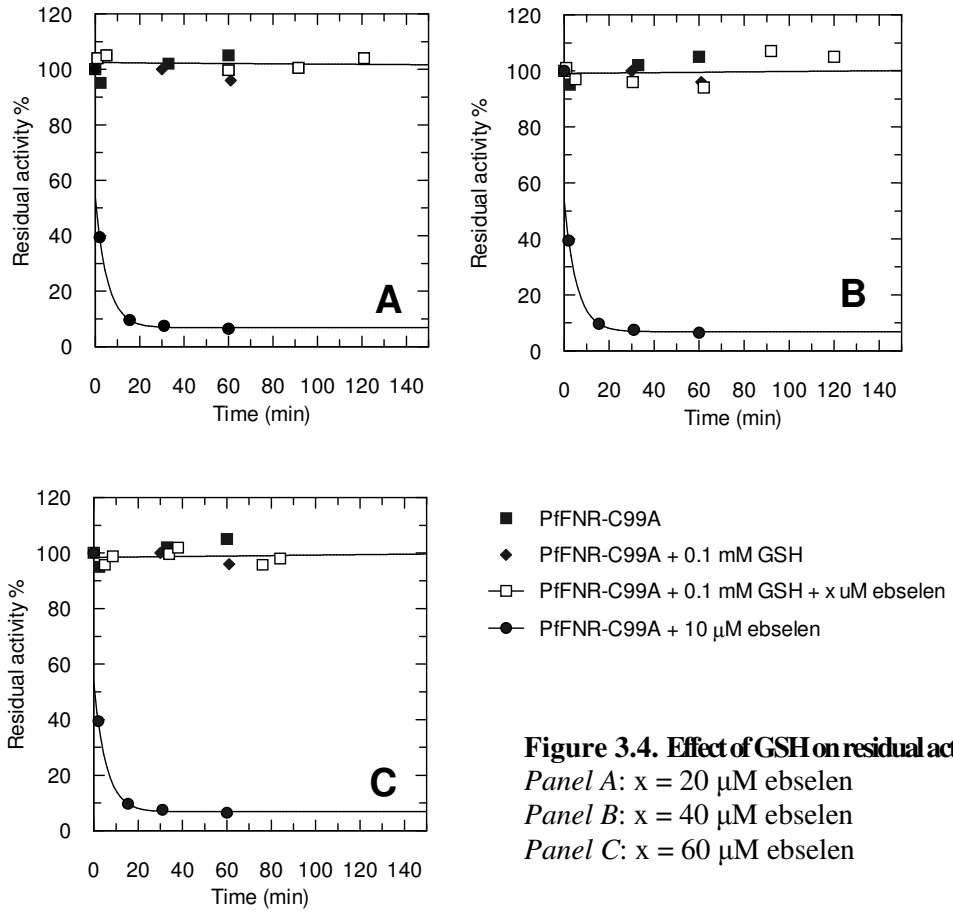

Figure 3.4. Effect of GSH on residual activity of PfFNR-C99A.
Panel A: x = 20 μM ebselen
Panel B: x = 40 μM ebselen
Panel C: x = 60 μM ebselen

3.1.2.3 KINETICS OF EBSELEN INHIBITION OF PfFNR

In order to study the inhibition mechanism of ebselen, I monitored the NADPH-dependent reduction of potassium ferricyanide in presence of different concentrations of inhibitor. The time courses of the reaction (Figure 4.5) were fitted with curves describing a slow onset of complete enzyme inhibition during the assay, according to a single exponential decay. The plots of each first-order rate constant (k_{obs}) versus ebselen concentration (Figure 4.6) allowed to calculated a second-order rate constant of PfFNR inactivation ($k_{ebselen}$) of $2.06x10^{-3}$ μM^{-1} s^{-1}. Since at a pH lower than 8 cysteine side chain should be protonated and less reactive, I evaluated PfFNR-C99A inhibition at pH 7.0 (Figure 4.6) yielding a 7-fold lower $k_{ebselen}$.

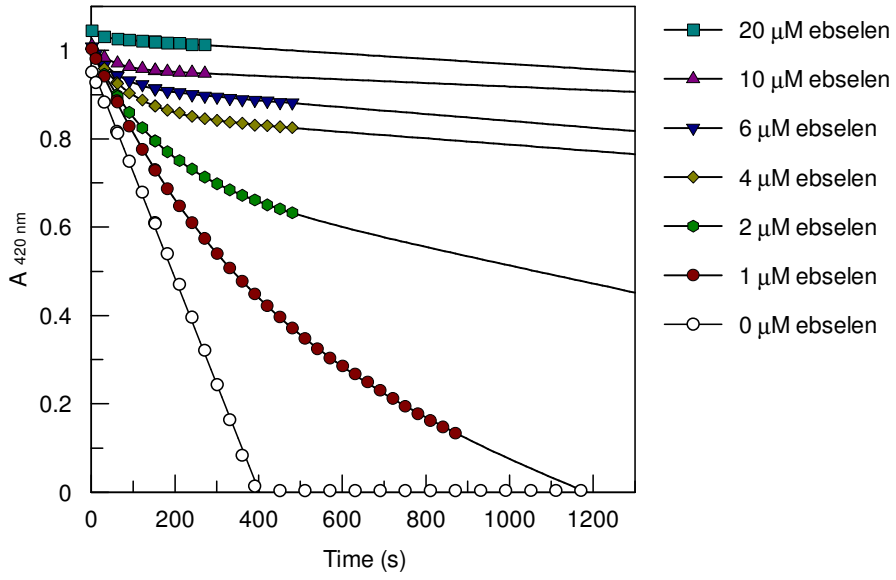

Figure 3.5. Effect of ebselen on the time course of NADPH-$K_3Fe(CN)_6$ reductase reaction catalyzed by PfFNR-C99A at pH 8.2

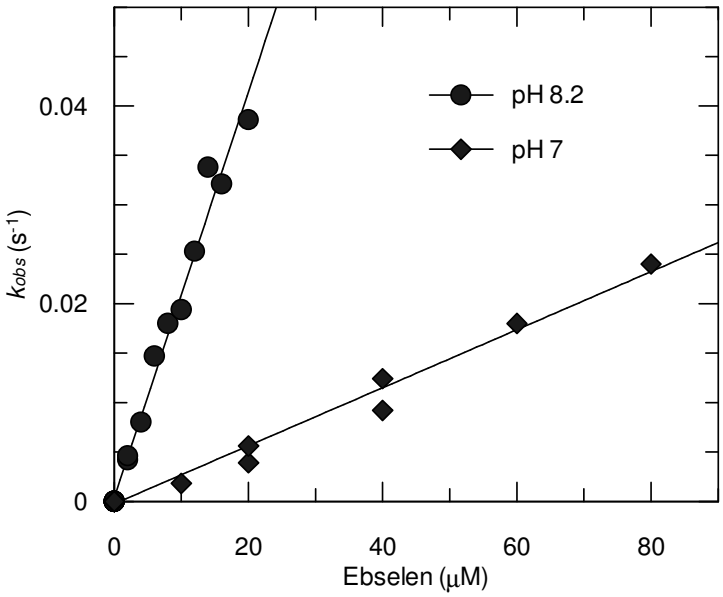

Figure 3.6. Secondary plot of the inactivation process showing the dependance of k_{obs} by ebselen concentration either at pH 8.2 or pH 7. The slope of each interpolating line represents the second order constant ($k_{ebselen}$).

3.1.2.4 SENSITIVITY OF DIFFERENT FNRs TO EBSELEN

In order to evaluate the specificity of ebselen, I studied its effect on wild type *Spinacia oleracea* (spinach) FNR (SoFNR), a plant homologue of PfFNR, and on *Mycobacterium tuberculosis* FprA, a ferredoxin reductase unrelated to PfFNR. As shown in Figure 4.7, FprA is completely resistant to ebselen. On the contrary SoFNR is inactivated by ebselen, although with a second order rate constant ($k_{ebselen}$) 10-fold lower than that of PfFNR (Figure 3.8 and Table 3.7). Moreover both PfFNR and SoFNR possesses in the active site a conserved cysteine residue, respectively Cys284 and Cys272, involved in the interaction with the substrate NADP(H). Interestingly the enzyme variant SoFNR-C272S is resistant to ebselen inactivation suggesting that Cys284 of PfFNR is possibly involved in the inactivation process.

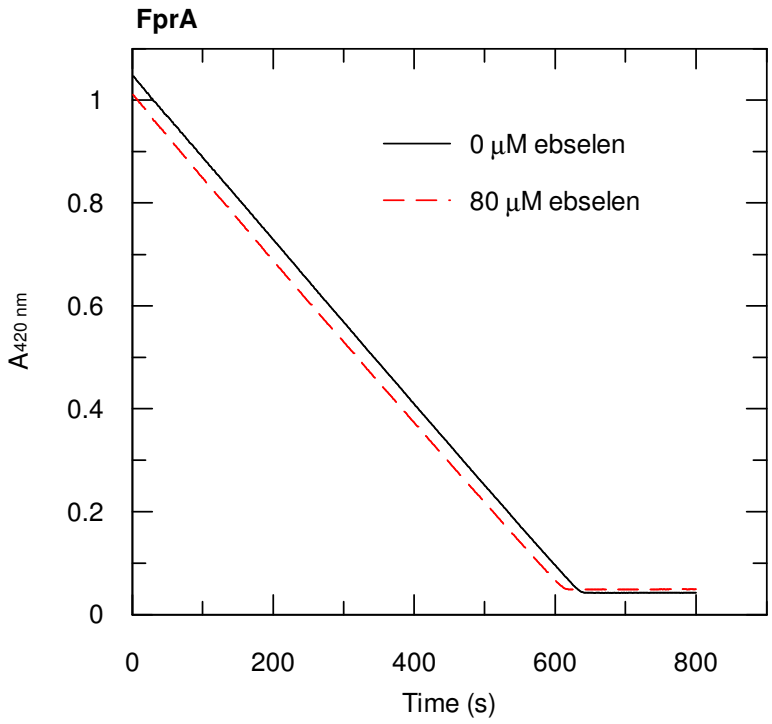

Figure 3.7. Effect of ebselen on time course of NADPH-$K_3Fe(CN)_6$ reductase reaction catalyzed by FprA.

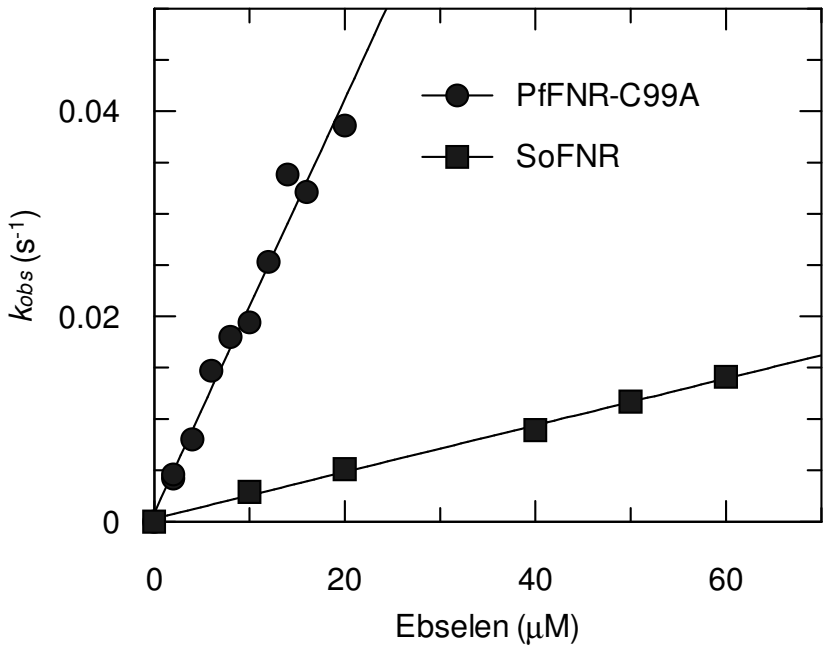

Figure 3.8. **Secondary plot of the inactivation process showing the dependance of k_{obs} by ebselen concentration at pH 8.2 determined for PfFNR-C99A and SoFNR.** The slope of each interpolating line represents the second order constant ($k_{ebselen}$).

Table 3.7. Values of second order rate constant of inactivation.

	$k_{ebselen}$ (s^{-1} μM^{-1})
PfFNR-C99A	0.00206 ± 0.00006
SoFNR	0.00022 ± 0.00002

3.1.2.5 PROTECTIVE EFFECT OF NADPH ON EBSELEN INACTIVATION

The hypothesis of a potential involvement of Cys284 in ebselen inactivation process suggested to test if NADPH may protect PfFNR from inactivation. The reduction of ferricyanide by PfFNR-C99A was monitored in presence of ebselen at various NADPH concentrations. The secondary plot of the inactivation process clearly points out a partial protective effect of NADPH on PfFNR with respect to ebselen inactivation (Figure 3.9).

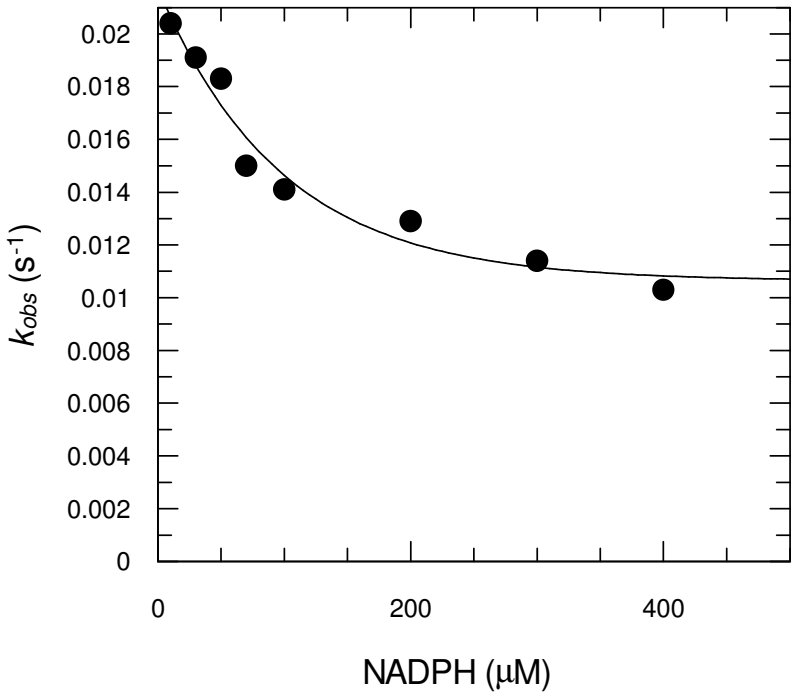

Figure 3.9. **Secondary plot of the inactivation process showing the decrease of k_{obs} at the increase of NADPH concentration.**

3.1.2.6 EFFECT OF Cys284Ser SUBSTITUTION ON PfFNR INHIBITION

In order to directly investigate the role of Cys284 of PfFNR on inactivation by ebselen, I purified the enzyme variant PfFNR-C99A/C284S. The substitution of Cys284 with a serine gave an enzyme with a residual activity sufficient to study its inactivation. As expected for the variant PfFNR-C99A/C284S, the activity measured as U/FAD (μmol product/μmol FAD/min) was about the 10% of that measured for the wild type enzyme (Table 3.8).

Table 3.8. Comparison between wt PfFNR and PfFNR-C99A/C284S activity.

NADPH-$K_3Fe(CN)_6$ reductase activity	
	U/FAD
wt PfFNR	5400
PfFNR-C99A/C284S	400

At pH 8.2 the effect of the substitution Cys284Ser on ebselen inhibition resulted to be negligible whereas at pH 7 the second order rate constant ($k_{ebselen}$) of PfFNR-C99A/C284S inactivation is lower than that of PfFNR-C99A, even if only about 2-fold (Table 3.9).

Table 3.9. Values of second order rate constant of inactivation

	$k_{ebselen}$ (s^{-1} μM^{-1})	
	pH 7	pH 8.2
PfFNR-C99A	0.000294 ± 0.000009	0.002056 ± 0.000062
PfFNR-C99A/C284S	0.000122 ± 0.00001	0.002359 ± 0.000033

3.1.2.7 EFFECT OF EBSELEN ON FLAVIN FLUORESCENCE

FAD is the prosthetic group of PfFNR and it is responsible of the enzyme spectral properties. Flavin fluorescence is measured as emission wavelength at 530 nm after an excitation at 450 nm and it is almost completely quenched by the interaction between apoenzyme and fluorophore. Figure 3.10 shows that the treatment of PfFNR-C99A with ebselen leads to dramatic increase of FAD fluorescence. Ultrafiltration of the enzyme treated with inhibitor for good showed that the increase in flavin fluorescence is due to the dissociation of flavin cofactor from the holoenzyme consistently with the irreversible inhibition mechanism of ebselen. Replacement of the active-site Cys284, a residue located in proximity of isoalloxazine ring of FAD, with a Ser made PfFNR much more resistant to ebselen-induced deflavinylation indicating that Cys284 is an important target of ebselen. A calculation of a rate constant for FAD dissociation was made impossible because of the complexity of fluorescence time courses. Nevertheless I deduced an half-life of the process by measuring the time required to obtain the release of 50% of FAD from enzyme (Table 3.10).

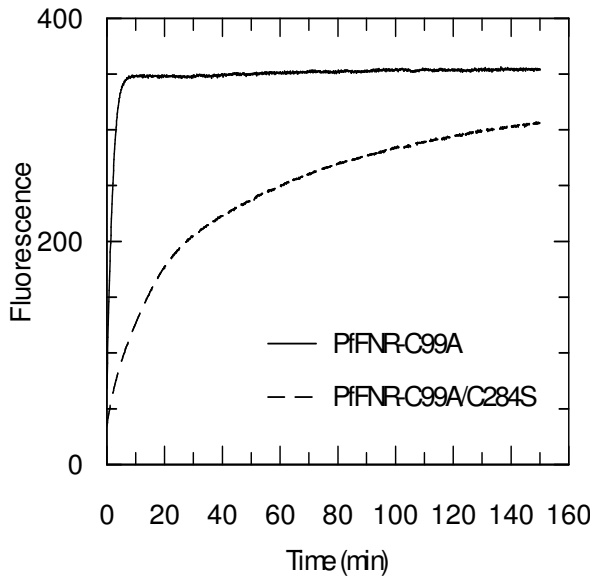

Figure 3.10. **Increase in FAD induced by ebselen.** PfFNR-C99A was treated with 20 μM ebselen at pH 8.2 (solid line) and PfFNR-C99A/C284S was treated with 20 μM ebselen at pH 8.2 (dashed line).

Table 3.10. Kinetic parameters for the deflavinylation of different PfFNR forms.

Time release of 50% of FAD (s)				
	pH 7		pH 8.2	
Ebselen	10 µM	20 µM	10 µM	20 µM
PfFNR-C99A	645	231	66	60
PfFNR-C99A/C284S	1620	1224	840	693

The comparison of 50% FAD time release with half-life of inactivation process (Table 3.11) points out that the process of FAD release is slower than enzyme inactivation suggesting that ebselen inhibition mechanism consisting in two separate phases. A first step of inactivation consisting of a rapid modification of one or more cysteine residue followed by a second slower step in which the modification of further cysteines causes the alteration of enzyme tridimensional structure. As an alternative, a rapid modification of cysteine residues causes either enzyme inactivation or a destabilization of protein conformation leading to FAD release. Moreover the replacement of Cys284 with a Ser has only a poor effect on PfFNR inactivation but it has a dramatic effect in enzyme deflavinylation caused by ebselen. Indeed the dissociation process of prosthetic group of PfFNR-C99A/C284S is 10 fold slower than that of PfFNR-C99A.

Table 3.11. Half-life of PfFNR inactivation process by ebselen.

Half-life (s)				
	pH 7		pH 8.2	
[Ebselen]	10 µM	20 µM	10 µM	20 µM
PfFNR-C99A	240 ± 7	118 ± 4	34 ± 1	17 ± 0.5
PfFNR-C99A/C284S	570 ± 47	290 ± 23	30 ± 0.4	15 ± 0.2

3.1.2.8 EBSELEN TARGETS THE Cys RESIDUES OF PfFNR

In order to evaluate the number of cysteine residues of PfFNR involved in the ebselen mechanism of action, I evaluated its effect on three variants of *Plasmodium falciparum* FNR: wild type PfFNR, PfFNR-C99A and PfFNR-C99A/C284S containing respectively 6, 5 and 4 cysteine residues. I incubated the enzyme with different ebselen concentrations corresponding to an inhibitor/enzyme molar ratio between 0.5:1 and 10:1. Figure 3.11 shows that the complete enzyme inactivation was obtained at a very low ebselen:enzyme molar ratio consistently with an irreversible mechanism of inhibition. Moreover the mutations that replaced either Cys99 (a known solvent-accesible residue) and Cys284 (a known residue involved in catalysis) decreased the molar ratio required to completely inactivate the enzyme indicating that both the residues Cys99 and Cys284 are targets of ebselen. The Figure 3.11 also suggests that, in addition to Cys99 and Cys284, at least two more Cys residues of PfFNR are targeted by ebselen.

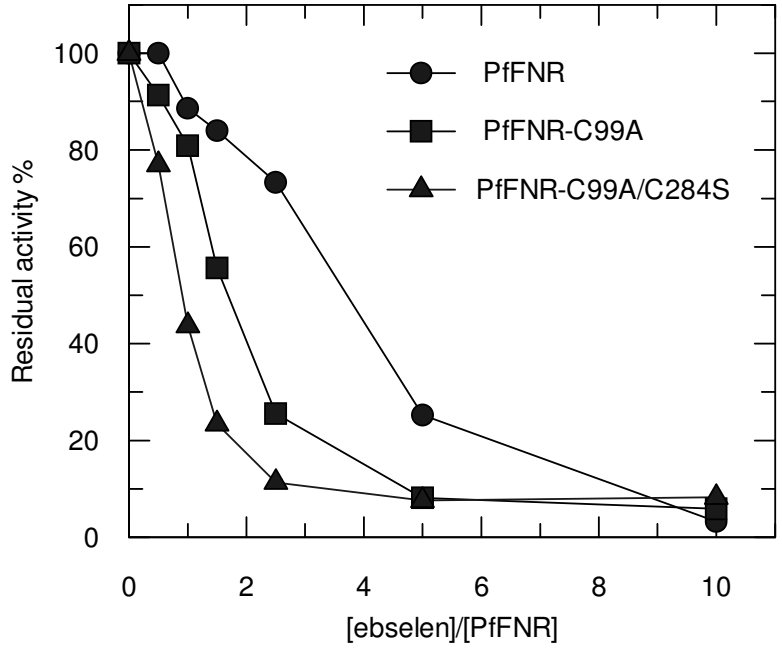

Figure 3.11. **Residual activity of different variants of PfFNR determined at the end-point of inactivation by different amounts of ebselen.**

3.2 OVERPRODUCTION AND PURIFICATION OF PfFNR-C99A AS CLEAVABLE FUSION WITH SUMO PROTEIN

In order to make easier in-depth studies on structure-function relationships in PfFNR, large amounts of recombinant protein are required. The expression and purification procedure previously developed (Balconi *et al.*, 2009) is quite expensive because of the cost of the factor Xa required to generate the mature PfFNR forms. In order to eliminate the need of commercial proteolytic enzymes, I developed a new *E. coli* expression system for PfFNR, based on the fusion with the yeast SUMO protein (pET SUMO system, Invitrogen), which can be removed with a protease that can be easily produced in the laboratory in recombinant form. The plasmid pETSUMO-PfFNR-C99A was constructed and found to produce detectable amount of soluble recombinant protein in Rosetta (DE3) *E. coli* cells. As shown in Table 3.12, the specific activity in trasformed cells is significantly higher than in those untransformed. Moreover I observed the maximum value of specific activity after 24 hours of induction. This result is confirmed by SDS-PAGE analysis which shows a similar improvement of the amount of protein with the highest expression level after 24 hours of induction. (Figure 3.12).

Table 3.12. **Expression of poly-His-SUMO-PfFNR-C99A in *E. coli* at 20 °C. Effect of induction time.**

	Induction time (hrs)	**Protein/ml (mg/ml)**	**Activity (U/ml)**	**Specific activity (U/mg)**
untransformed	*3 h*	15.5	12.7	0.82
	6 h	23.8	12.9	0.54
	21 h	26.7	15.8	0.59
	24 h	24.6	13.9	0.57
transformed	*3 h*	9.2	7.8	0.85
	6 h	11.5	9.2	0.80
	21 h	22	26.5	1.2
	24 h	21.4	25.6	1.2

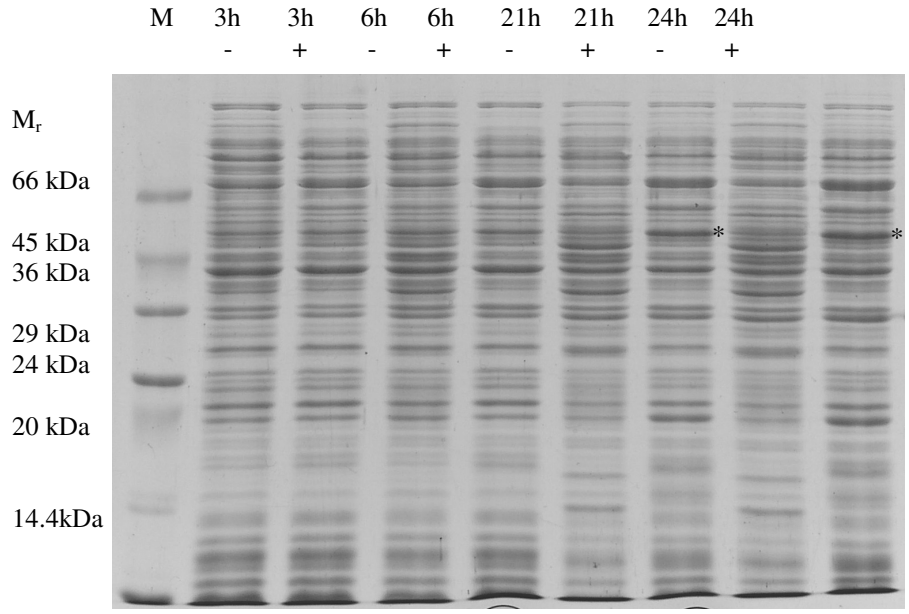

Figure 3.12. **Expression of poly-His-SUMO-PfFNR-C99A at 20 °C.**
SDS-PAGE analysis of soluble extracts of uintransformed (-) and transformed (+) cells with plasmid pETSUMO-PfFNR-C99A at different hours after induction with IPTG. Each sample contains 30 µg total proteins. Lane M, molecular mass markers (mass value are reported on the left). An asterisk is placed on the right of the band of poly-His-SUMO-PfFNR-C99A.

Since the protein contains an N-terminal tag of histidines, I isolated poly-His-SUMO-PfFNR-C99A using a nickel-chelate chromatography as the initial purification step (Figure 3.13A). Incubation with poly-His-Senp2 protease of partially purified poly-His-SUMO-PfFNR-C99A resulted in a rapid cleavage to two fragments. A second purification step of nickel-chelate chromatography was performed in order to separate the protein from both protease and the residual uncleaved protein (Figure 3.13B). This second step was made possible by the affinity, altough weak, of the cleaved protein for the resin.

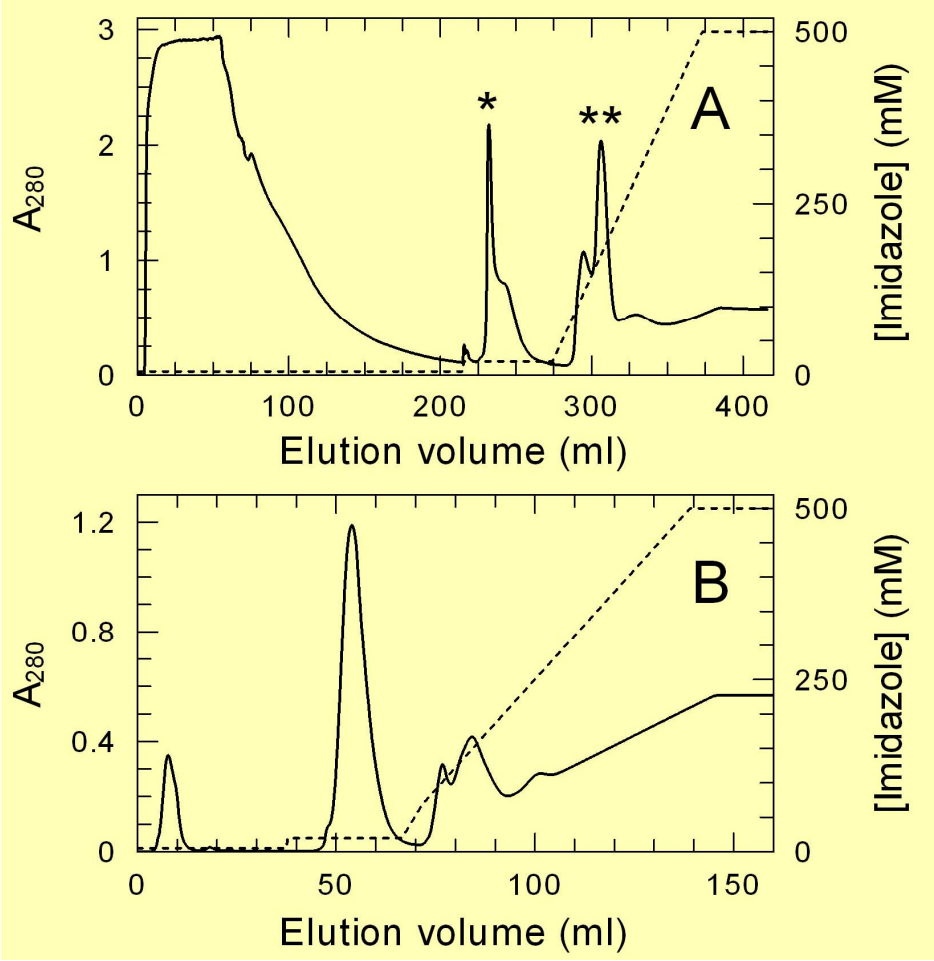

Figure 3.13A and 3.13B. Chromatograms of the two separation steps of PfFNR-C99A purification.

It's interesting to note that the first nickel-chelate chromatography also yielded, at low concentration of imidazole, a truncated form of the recombinant protein with a molecular weight not much different from that of PfFNR-C99A (Figure 3.14). On the basis of this observation I hypothesized that this protein could be generated by an *in vivo* partially spontaneous splitting of poly-His-SUMO-PfFNR-C99A. The hypothesis of an *in vivo* cleavage was supported by immunoblot analysis (Figure 3.15) with anti-PfFNR antibodies which indicates that shortened forms of the recombinant protein are produced in *E. coli*, possibly by proteolysis. The identity of this truncated protein and the integrity of the final product PfFNR-C99A have been verified by N-terminal sequencing. The major truncated protein resulted to lack of the two initial residues, Ser and Met, starting at Gly (-1), instead of the mature PfFNR-C99A which resulted to have the expected sequence starting at residue Ser (-3), indicating a proper cleavage of the fusion protein. The purification protocol yielded about 0.2 milligrams of PfFNR-C99A per gram of cells with a global yield of 28%. Table 3.13 and Figure 3.14 shows the achievement of PfFNR-C99A purification highly homogeneous and suitable for structural and functional characterization.

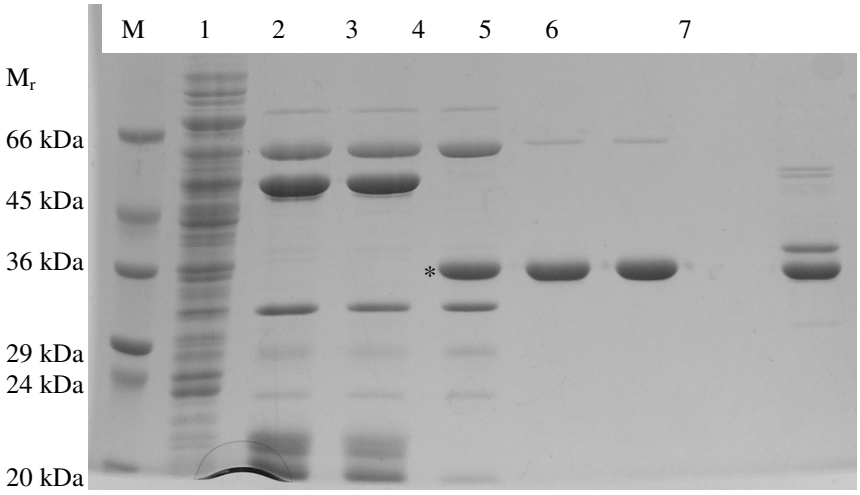

Figure 3.14. **SDS-PAGE analysis of PfFNR-C99A purification.**
Lane M, molecular mass markers; **lane 1**, soluble extract containing 30 µg total proteins; **lane 2**, poly-His-SUMO-PfFNR-C99A after Ni Sepharose HP; **lane 3**, after buffer change by gel filtration; **lane 4** after digestion with polyHis-Senp2 protease (PfFNR-C99A cleaved is marked with an asterisk); **lane 5**, after the second chromatographic step on Ni Sepharose HP; **lane 6**, after buffer change by gel filtration; **lane 7**, PfFNR-C99A obtained by spontaneous proteolysis.

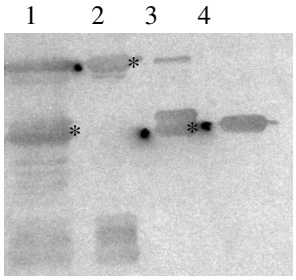

Figure 3.15. **Western blot immunostained using an anti-PfFNR antibody**. **Lane 1**, analysis on soluble extracts (spontaneously cleaved PfFNR-C99A is marked with an asterisk). **Lane 2**, poly-His-SUMO-PfFNR-C99A (marked with an asterisk); **lane 3**, spontaneously cleaved PfFNR-C99A (marked with an asterisk); **lane 4**, PfFNR-C99A.

Table 3.13. **Purification table of PfFNR-C99A.**

Step	Volume (ml)	Protein (mg)	A_{280}/A_{454}	FAD (nmoli)	Activity (U)[a]	Specific activity (U/mg)[a]	Yield (%)	Purification (fold)
crude extract	180	2880	/	/	6400	2.22	100	1
Ni Sepharose	17.6	105	9.5	450	1660	15.8	26	7.12
Ni Sepharose	4.75	11.7	6.9	323	1810	155	28	69.8

[a] NADPH-$K_3Fe(CN)_6$ reductase activity

3.3 PfFNR MUTANT FORMS

In order to probe the role of His286 and Lys249 in the catalytic mechanism of PfFNR and in binding the substrate, I produced and characterized a series of mutant enzymes in which His286 was changed to Ala, Gln, Lys, or Leu, and Lys249 was replaced with Ala.

3.3.1 PfFNR FORMS OVERPRODUCTION AND PURIFICATION

Either the substitution of His286 with Ala, Gln, Lys and Leu or the substitution of Lys249 with Ala yielded mutant PfFNR forms that were produced in *E. coli* Rosetta (DE3) and purified according to the protocol optimized for the wild type enzyme (Balconi *et al.*, 2009). His286 and Lys249 did not reveal a relevant role in protein folding and stability since each enzymatic variant were purified to an homogeneity and with a yield comparable to that of wild type PfFNR. Moreover mutations in His286 and Lys249 did not alter the ability of the enzyme to weakly bind to the nickel chelate resin after the removal of His-tag ruling out a role for His286 and Lys249 in determining the affinity for nickel ion. All the variants did not display differences in extinction coefficient and spectral features from those of wild type PfFNR, indicating that the engineered mutations do not perturb the conformation of the protein.

3.3.2 CATALYTIC PROPERTIES OF His286 MUTANTS OF PfFNR

The kinetic parameters of PfFNRs mutant forms have been determined for NADPH-dependent diaphorase activities. As shown in Table 3.14, the effect of the mutations on the steady-state kinetic parameters for the NADPH-$K_3Fe(CN)_6$ reductase reaction is strongly dependent on which residue is replacing His286. With the exception of the His286Gln replacement, which slightly increases k_{cat}, all the other mutations significantly decrease both k_{cat}/K_m^{NADPH} and k_{cat}. The interpretation of these data is made difficult because ferricyanide ion, besides being an artificial substrate, is a competitive inhibitor of PfFNR with respect to NADPH. Then I have also determined the kinetic parameters using the artificial electron acceptor DCPIP, which does not inhibit PfFNR. The kinetic properties of PfFNR mutants measured with DCPIP are in good agreement with those observed using ferricyanide (Table 3.15). Notably, in the NADPH-DCPIP reductase reaction, the mutation His286Gln, besides slightly increasing k_{cat}, strongly increases k_{cat}/K_m^{NADPH}. Moreover all

the other aminoacid substitutions negatively affect both k_{cat}/K_m^{NADPH} and k_{cat} (Table 3.15). Unexpectedly, steady-state kinetics indicated that the His286Leu mutation determines the largest decrease in k_{cat}/K_m^{NADPH}, while mutation His286Lys yields the mutant enzyme with the lowest k_{cat} when ferricyanide is the electron acceptor (Table 3.14). This evidence demonstrates that Leu, a residue commonly found at this site in other plastidic-type FNRs, and Lys, which carries a positive charge suitable for the interaction with NADP(H) pyrophosphate, are not substitutes for His286 in PfFNR. 2'-P-AMP acts on PfFNR forms as competitive inhibitor with the substrate NADPH. I evaluated the role of His286 side chain in binding the adenylate moiety of the substrate by measuring the inhibition constant displayed by 2'-P-AMP ($K_i^{2'\text{-P-AMP}}$). $K_i^{2'\text{-P-AMP}}$ values can be taken as a rough estimate of the dissociation constant of the complexes between the PfFNR forms and the inhibitor. Table 3.16 shows that the values of $K_i^{2'\text{-P-AMP}}$ of the mutant PfFNRs well compare with those of K_m^{NADPH} in the diaphorase reactions (Table 3.14 and 3.15). PfFNR-H286A shows the lowest affinity for the ligand, while PfFNR-H286Q is the form most similar to the wild-type enzyme. Interestingly, PfFNR-H286K displays an affinity for 2'-P-AMP 8-fold higher than that of the wild-type PfFNR.

Table 3.14. Kinetic parameters of PfFNR forms in the NADPH-$K_3Fe(CN)_6$ reductase reaction

PfFNR form	k_{cat} (e- equiv s^{-1}) (%)	K_m^{NADPH} (μM)	k_{cat}/K_m^{NADPH} (e- equiv s^{-1} μM^{-1}) (%)	$K_i^{K_3Fe(CN)_6}$ (μM)
wild type	250 ± 8 (100)	36 ± 6	7.0 ± 1 (100)	230 ± 40
H286Q	370 ± 6 (150)	57 ± 5	6.5 ± 0.6 (93)	110 ± 11
H286K	7.6 ± 0.4 (3)	nd[a]	nd[a]	nd[a]
H286A	89 ± 2 (36)	520 ± 55	0.17 ± 0.01 (2.4)	91 ± 11
H286L	15 ± 0.6 (6)	370 ± 46	0.04 ± 0.005 (0.6)	91 ± 15

[a]Not determinable. A reliable estimate of K_m^{NADPH} was not possible because of the apparently very low value of $K_i^{K_3Fe(CN)_6}$ for the PfFNR-H286K mutant.

Table 3.15. Kinetic parameters of PfFNR forms in the NADPH-DCPIP reductase reaction

PfFNR form	k_{cat} (e- equiv s^{-1}) (%)	K_m^{NADPH} (μM)	k_{cat}/K_m^{NADPH} (e- equiv s^{-1} μM^{-1}) (%)
wild type	110 ± 3 (100)	71 ± 4	1.5 ± 0.1 (100)
H286Q	140 ± 11 (130)	22 ± 3	6.3 ± 0.9 (420)
H286K	12.0 ± 0.7 (11)	140 ± 14	0.09 ± 0.001 (5.8)
H286A	35.0 ± 1.7 (32)	400 ± 40	0.098 ± 0.009 (6.5)
H286L	nd[a]	nd[a]	nd[a]

[a]Not determinable. The kinetic parameters were not measured because of an anomalous reactivity of PfFNR-H286L with DCPIP.

Table 3.16. Parameters for the inhibition by 2'-P-AMP of the PfFNR forms in the NADPH-DCPIP reductase reaction [a]

PfFNR form	$K_i^{2'\text{-P-AMP}}$ (μM)
wild type	24 ± 2
H286Q	71 ± 7
H286K	2.9 ± 0.2
H286A	230 ± 25

[a] The $K_i^{2'\text{-P-AMP}}$ of PfFNR-H286L was not determined because of an anomalous reactivity of this mutant enzyme with DCPIP.

3.3.3 BINDING OF $NADP^+$

In order to further investigate the role of His286 in the stabilization of the enzyme-substrate complex, I studied the interaction of the PfFNR forms with $NADP^+$ by differential spectrophotometry. It is known that $NADP^+$ binding to plastidic-type FNR induces perturbation in the visible region of the protein-bound FAD spectrum. Furthermore, it has been demonstrated that the positive peak around 500 nm in the difference spectrum (Figure 3.16B) is due to the stacking interaction between the nicotinamide of $NADP^+$ and the isoalloxazine ring of FAD (Piubelli *et al.*, 2000). Thus this experiment provides both the information about the K_d for $NADP^+$ and the position of its nicotinamide ring within the complex. The K_d values of the $NADP^+$ complexes are comparable with the K_i of 2'-P-AMP, showing similar trends. Figure 3.16A shows the titration curves of PfFNR forms with $NADP^+$ indicating the fraction of bound enzyme versus the relative concentration of $NADP^+$. The difference spectra in the visible region of the $NADP^+$-saturated PfFNR forms are markedly different from that of the wild-type enzyme (Figure 3.16B). In PfFNR-H286Q, the positive peak centered at 504 nm is much more intense than that observed with PfFNR. On the other hand, substitutions of His286 with Ala and Lys led to enzyme forms whose $NADP^+$-complexes displayed a negative peak at this wavelength. These observations indicates that the positioning of the nicotinamide ring of $NADP^+$ in proximity to the isoalloxazine ring of FAD is stronlgy impaired by substitutions in Ala and Lys, whereas is stabilized by substitution in Gln. This conclusion is also supported by the values of k_{cat} since the stacking interaction nicotinamide-isoalloxazine is an essential requirement for the HT. Only for the mutant PfFNR-H286K the increase of the affinity for $NADP^+$ is related to a destabilized interaction between nicotinamide of $NADP^+$ and isoalloxazine ring of FAD.

Table 3.17. Parameters for K_d values of the complexes between PfFNR and NADP$^+$ [a]

PfFNR form	K_d^{NADP+} (μM)
wild type	60 ± 9
H286Q	130 ± 10
H286K	30 ± 5
H286A	280 ± 90

[a] The very small spectral changes induced by binding of NADP$^+$ to PfFNR-H286L prevented a reliable estimate of the K_d value of the resulting complex.

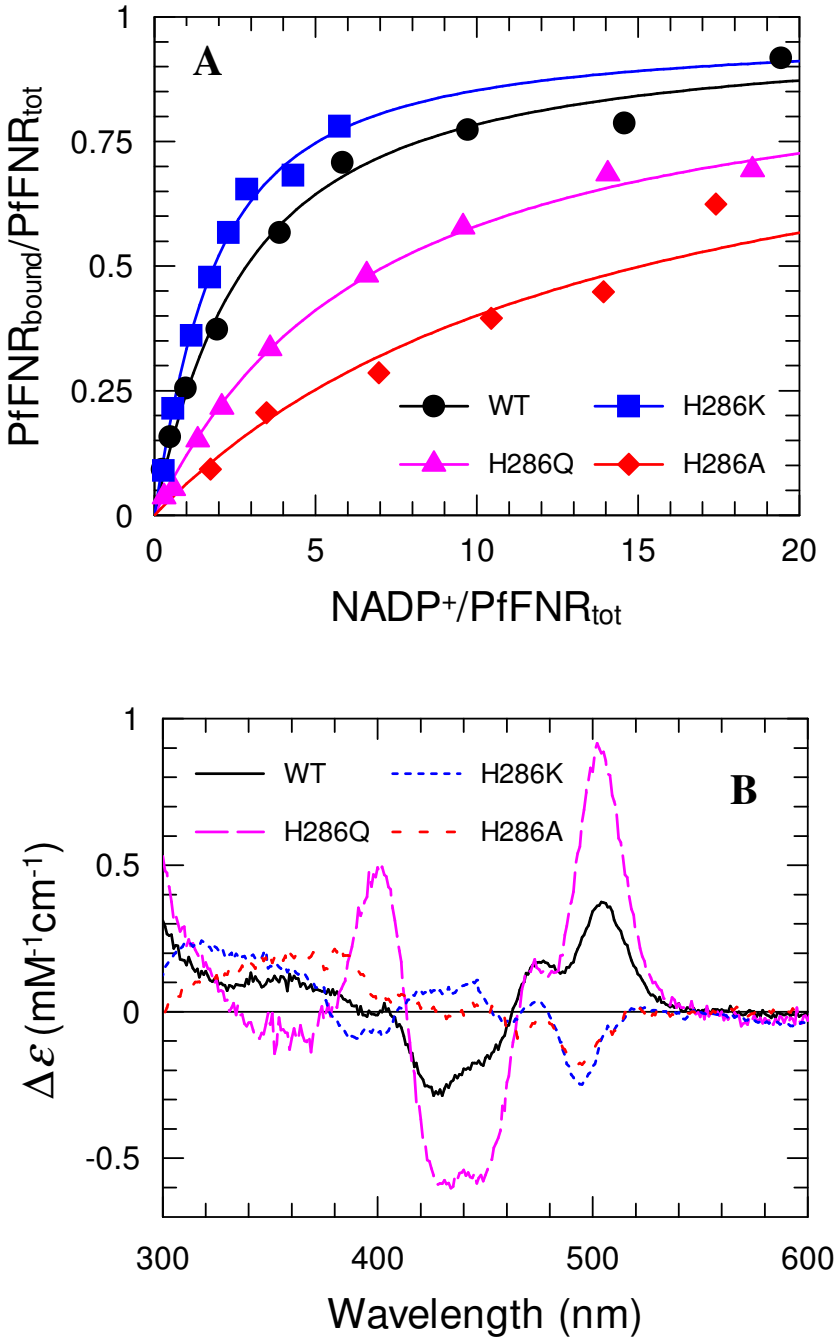

Figure 3.16 A. Complex formation between PfFNR forms and NADP$^+$. Titration curves obtained by successive additions of NADP$^+$ to solutions of wild-type PfFNR, PfFNR-H286K, PfFNR-H286Q and PfFNR-H286A at 15 °C. PfFNR forms were diluted in 50 mM Tris-HCl, pH 7.6.Curves represent the theoretical eqution for 1:1 protein-ligand binding model drawn using K_d and Δε parameters obtained by nonlinear fitting of experimental data as described in Materials and Methods section 2.9. **B. Difference spectra of enzyme-NADP$^+$ complexes.** Difference spectra of the complexes of wild-type PfFNR are extrapolated at infinite NADP$^+$ concentration.

3.3.4 PHOTOREDUCTION EXPERIMENTS

Photoreduction experiments under anaerobic conditions provide informations about the spectral properties of the flavin prosthetic group in its various redox states. Nicotinamide-flavin stacking interactions can be easily detected by the appearence of absorption bands above 600 nm, which are due to the formation of charge-transfer complexes between NADPH and FAD (CT1) and between $NADP^+$ and $FADH^-$ (CT2).

In order to verify if the change of His286 hampers or favors the HT-competent position of the nicotinamide, I performed stepwise anaerobic photoreductions of PfFNR-H286Q and PfFNR-H286K in presence of $NADP^+$. As in the case of wt PfFNR, the peak at 454 nm of bound FAD becomes almost completely bleached in mutant PfFNRs before NADPH starts to accumulate, as evaluated by the increase in absorbance at 340 nm. In the case of wt PfFNR a CT complex, most probably CT2, is clearly observed in the latest stages of photoreduction (Figure 3.17 A). In the case of PfFNR-H286Q the amount of CT was slightly but significantly higher (Figure 3.17 B). Conversely, CT absorption bands were not detected in PfFNR-H286K (Figure 3.17 C). These results confirm that the His286Gln mutation stbilizes the interaction between the redox-active moieties of bound NADP(H) and FAD, which is, instead impaired by the His286Lys mutation.

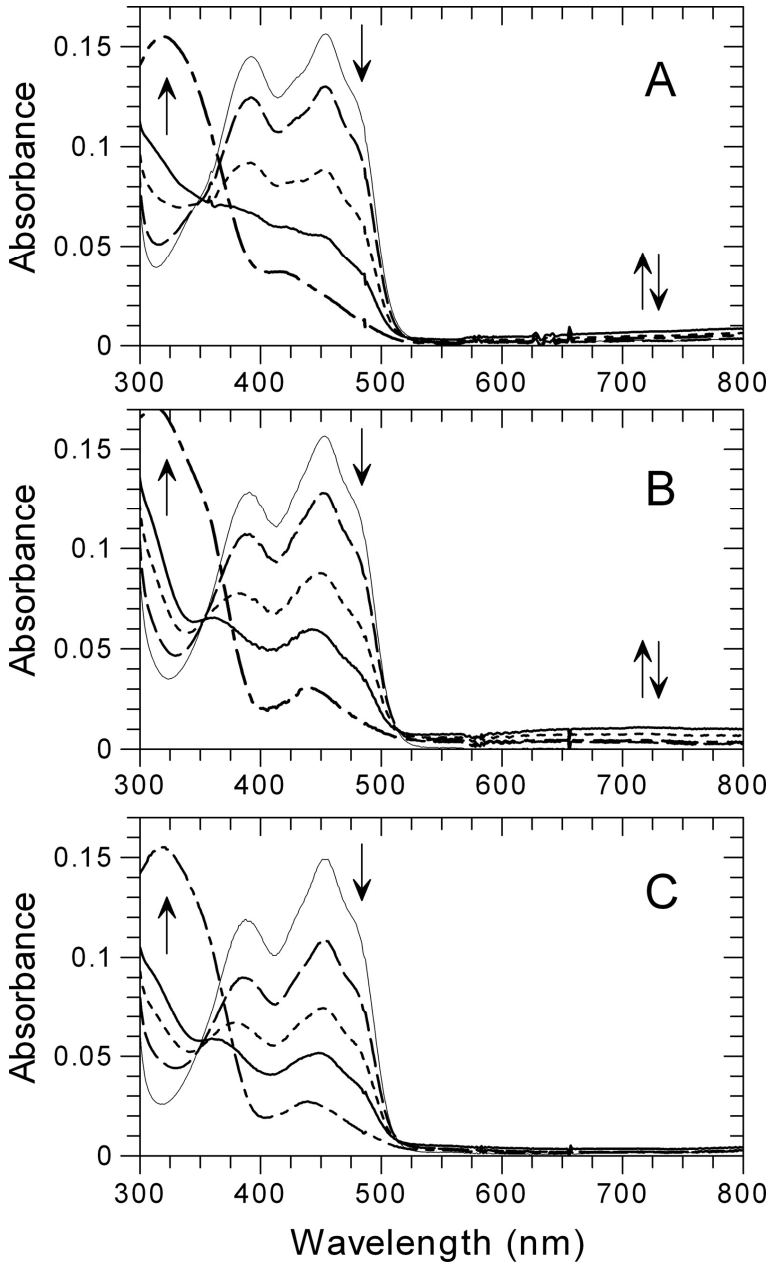

Figure 3.17. **Photoreduction in presence of $NADP^+$.** Absorbance spectra of anaerobic solutions of ~15 μM PfFNR (**A**), PfFNR-H286Q (**B**), and PfFNR-H286K (**C**) with 18 μM $NADP^+$ in 50 mM HEPES-NaOH, pH 7.0 containing 10% glycerol, recorded before (thin solid line) and after successive periods of illumination (1, 3, 5 and 12 min) with visible light. Arrows indicate the direction of the spectral changes.

3.3.5 RAPID REACTION STUDY OF THE REDUCTIVE HALF REACTION OF PfFNR-H286Q AND PfFNR-H286L WITH NADPH

In order to have a further proof of the effect of His286 replacement on HT from NADPH to FAD, two selected mutants, PfFNR-H286Q and PfFNR-H286L, were reacted at 25 °C with NADPH at concentration ranging from 25 μM to 1000 μM in comparison with wild-type enzyme. Absorbance data were collected over the entire 400-700 wavelength span of the diode-array detector. The composition of the reaction medium (50 mM HEPES-NaOH, pH 7.0) is different from that used for the steady-state parameters determination and this composition was chosen to allow a comparison with the recently obtained data for wild-type PfFNR. The time course of the reaction of the wild-type enzyme with 500 μM NADPH (after mixing) is shown in Figure 3.18A and 3.19A,B. Within the instrument dead-time, the transient formation of CT1 between NADPH and enzyme bound FAD occured, as judged from the high absorbance above 500 nm of the spectra recorded immediately after mixing, and from the value of absorbance at 454 nm, lower than expected for oxidized PfFNR (Figure 3.18A). The observable part of the reaction consisted in a further bleaching of the flavin main absorbance peak with a concomitant decrease of the absorbance band above 500 nm. The reaction of wild-type PfFNR with NADPH was previously described as a single-phase process with a rate constant essentially independent of NADPH concentration (Balconi E. *et al.*, 2009). Here I performed a more detailed analysis by extending the reaction time of > 100 ms, allowing the observation of two phases. I found a first phase with a k_{obs1} of ~150 s^{-1}, in which most of the absorption at 454 nm was lost corresponding to the HT step of the catalytic cycle. The process is followed by a second slower phase with a k_{obs} (k_{obs2}) of 8 s^{-1}, which accounts for ~10% of the total A_{454} change (Figure 3.18A and 3.19A). As expected on the basis of its higher k_{cat} values, PfFNR-H286Q was found to react with NADPH faster than the wild-type enzyme (Figure 3.18B and 3.19A). While the rate constant of the slow phase is essentially unchanged with respect to that of the wild-type enzyme, the k_{obs1} was found to be 240 s^{-1}, a value 1.7-fold higher than that of wt PfFNR (Figure 3.19C). Although more than half of the first fast phase occured in the dead time, the first spectra recorded 0.7 ms after mixing shows a broad band of absorbance above 500 nm which can be attribute to CT complexes and which is more intense than that recorded in the case e of the wild-type enzyme (Figure 3.18A and 3.18B). This observation suggests that the initial enzyme-NADPH complex has an higher CT character in the PfFNR-H286Q than in the wild-type enzyme, which most

probably represents the cause of the higher HT rate of the mutant PfFNR form. The reduction of the PfFNR-H286L differed from that of the wild-type PfFNR in three aspects. First, the fast phase of FAD bleaching occurs with a k_{obs1} of 44 s^{-1}, a value significantly slower than that of wt PfFNR, and, consistently with this low HT rate, the amount of CT complexes observed immediately after mixing was smaller (Figure 3.18 C). Second, the slower phase of the reaction with NADPH, although occurs with a rate similar to that of other PfFNR forms, accounts for ~50% of the total A_{454} change for NADPH concentrations > 100 μM (Figure 3.18C and 3.19C). The amplitude of slow phase was found to decrease as the NADPH concentration increasing, while that of the first phase was found to increase. In order to provide an explanation for this behavior, I proposed that the equilibrium between CT1 and CT2 is altered in PfFNR-H286L with respect to the wt enzyme, leaving a significant fraction of bound FAD in the oxidized form at the end of the first observable phase. Moreover, the spectral features of the species accumulating during the slow phase suggests the presence of blue semiquinone form of the flavin (Figure 3.18C) indicating that in this part of the process a reaction takes place between oxidized and reduced enzyme forms to yield the semiquinone species of bound FAD. Third, as shown in Figure 3.19C, the value of k_{obs1} displays a dependence on the NADPH concentration that is more marked than that observed with the two other enzyme forms, consistent with the higher values of K_m^{NADPH} of PfFNR-H2386L.

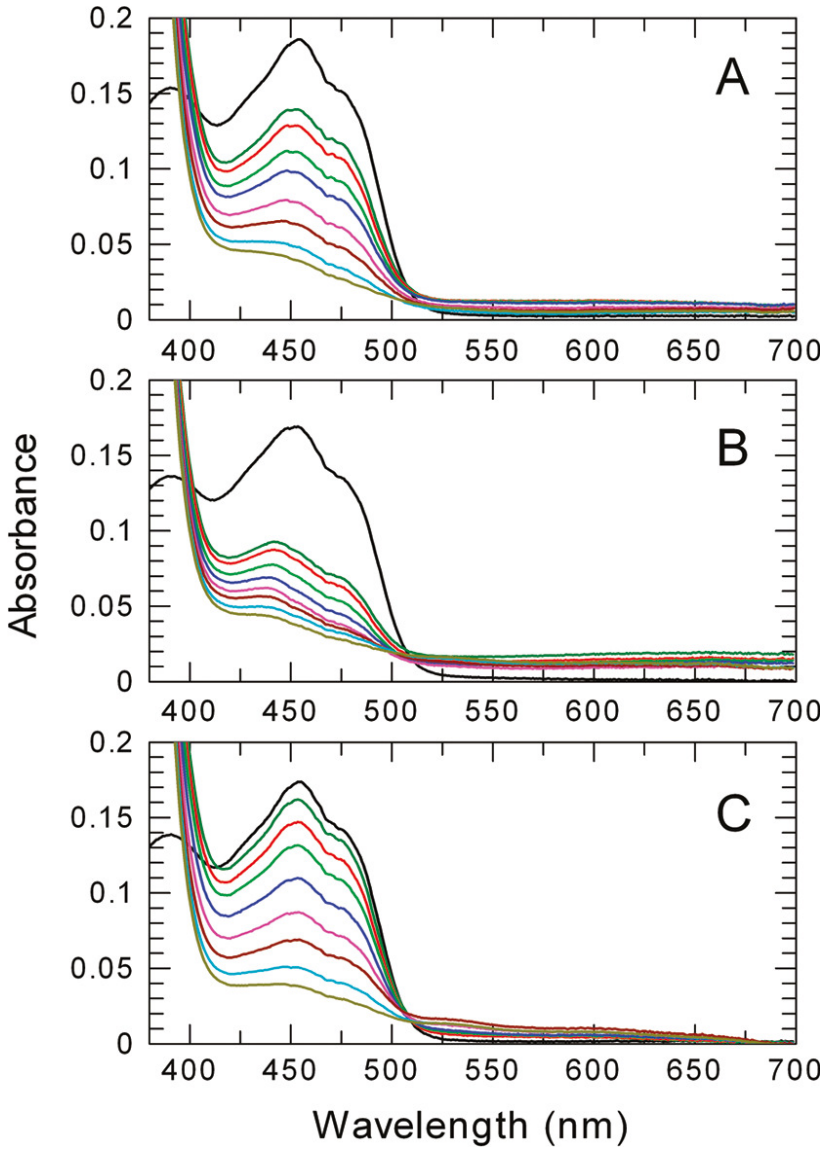

Figure 3.18. **Spectra recorded by stopped-flow during the anaerobic reduction of PfFNR forms (17-18 µM) by 500 µM NADPH (after mixing) at 25 °C in 50 mM HEPES-NaOH pH 7.0.**
A Spectrum of oxidized **PfFNR** (black) and those recorded 1 ms (dark green), 2 ms (red), 5 ms (light green), 7 ms (blue), 11 ms (magenta), 17 ms (brown), 61 ms (aqua) and 1 s (olive) after mixing.
B Spectrum of oxidized **PfFNR-H286Q** (black) and those recorded 0.7 ms (dark green), 2.2 ms (red), 3.7 ms (light green), 6.7 ms (blue), 11 ms (magenta), 32 ms (brown), 110 ms (aqua) and 450 ms (olive) after mixing.
C Spectrum of oxidized **PfFNR-H286L** (black) and those recorded 2.2 ms (dark green), 6.7 ms (red), 14 ms (light green), 29 ms (blue), 76 ms (magenta), 320 ms (brown), 1 s (aqua) and 2.9 s (olive) after mixing.

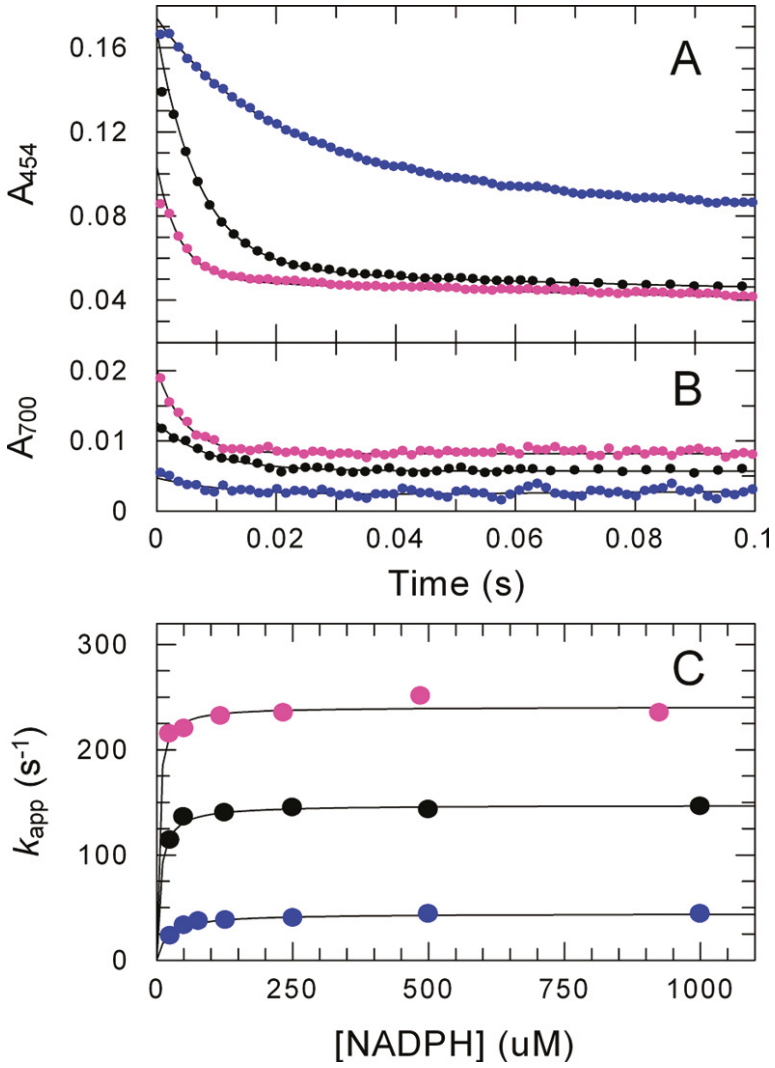

Figure 3.19. **Absorbance traces and NADPH concentration dependence of the reductive half-reaction of selected His286 mutants of PfFNR, as studied by stopped-flow spectrophotometry**. The PfFNR forms were reacted with NADPH at concentrations ranging from 25 μM to 1 mM (after mixing).
A. Absorbance at 454 nm recorded during the reaction of PfFNR (black). PfFNR-H286Q (magenta), and PfFNR-H286L (blue) with 500 μM NADPH.
B. Absorbance at 700 nm of the same reactions displayed in panel A.
C. Plot of the value of the rate constant of the fast phase of the reaction as a function of NADPH concentration (after mixing). Data from the three enzyme forms are identified by the same colors as those used in panels A and B. Fitting curves rectangular hyperbolae. Limiting values are 148 ± 2, 240 ± 4, and 44 ± 0.9 s^{-1} for wt PfFNR, PfFNR-H286Q and PfFNR-H286L, respectively.

3.3.6 pH DEPENDENCE OF k_{cat} and k_{cat}/K_m^{NADPH}

The pH dependence of the steady-state kinetic parameters of wild-type PfFNR were determined in the pH range 6.25-10.25, at varying concentrations of both NADPH and $K_3Fe(CN)_6$. The k_{cat} value is pH independent between pH 6.25 and 9.5, suggesting that there are not ionizable catalytic groups required for catalysis in this range of pH (Figure 3.20). Instead, the data about k_{cat}/K_m^{NADPH} values were fit with the equation describing a pH profile with an upper limiting value at low pH and a slope of -2, consisting with the requirement of two protonated groups important either for binding or catalysis (Figure 3.20). The apparent pK_a value determined for both the groups was 9.5 ± 0.04. In order to evaluate if His286 could be one of the ionizable groups responsible of the pH effect, I performed the pH profiles of the kinetic parameters with PfFNR-H286Q (Figure 3.21). The k_{cat} value is pH independent between pH 6.25 and 9.5 as well as previously determined for wild-type enzyme. Instead, the k_{cat}/K_m^{NADPH} values of PfFNR-H286Q were fit best with an equation describing a pH profile with an upper limiting value at low pH and a slope of -1. The apparent pK_a determined for the plot of k_{cat}/K_m^{NADPH} versus pH was 8.5 ± 0.01. This result indicates that His286 is most likely one of the two ionazable groups that is responsible for substrate binding in the wt enzyme, but not for catalysis since the k_{cat} is pH independent throughout all the pH investigated.

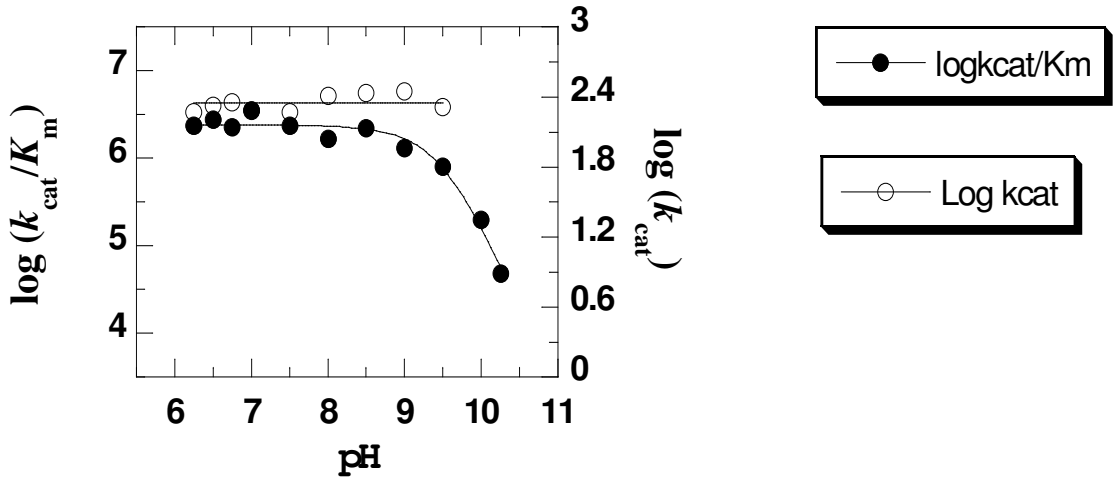

Figure 3.20. **pH dependence of the k_{cat} and k_{cat}/K_m^{NADPH} values for wild-type PfFNR.** Activity assays was measured at varying concentration of both NADPH and $K_3Fe(CN)_6$ between pH 6.25 and 10.25, at 25 °C.

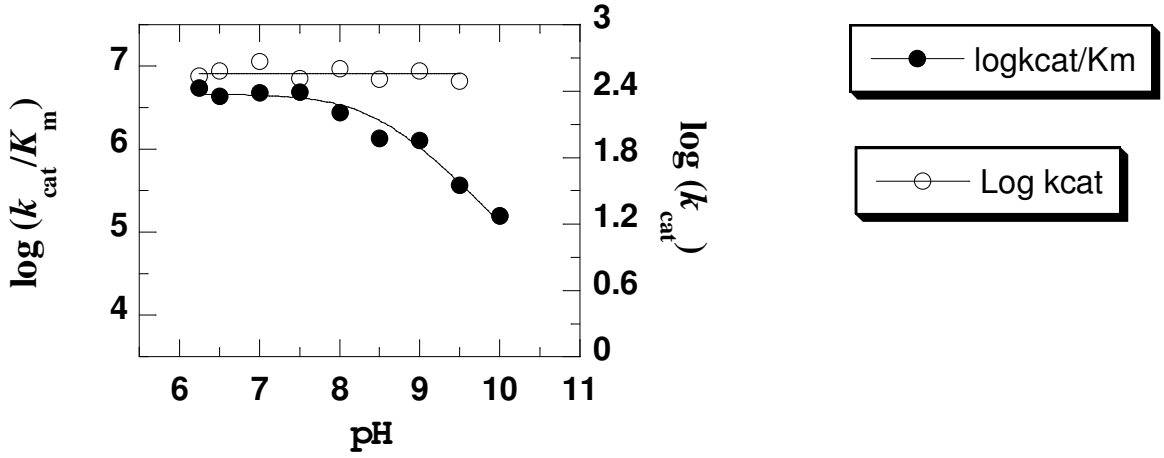

Figure 3.21. **pH dependence of the k_{cat} and k_{cat}/K_m^{NADPH} values for PfFNR-H286Q.** Activity assays was measured at varying concentration of both NADPH and $K_3Fe(CN)_6$ between pH 6.25 and 10, at 25 °C.

3.3.7 STRUCTURAL CHARACTERIZATION OF PfFNR-H286K AND PfFNR-H286L

Crystallization of PfFNR-H286L, PfFNR-H286L-2'P-AMP complex and PfFNR-H286K-2'-P-AMP was carried out in collaboration with Dr. Mario Milani, Università degli Studi di Milano, Milan, Italy. We obtained crystals that displayed overall structures very similar to their wild-type analogues obtained in absence and in presence of 2'-P-AMP (Milani M. *et al.*, 2007). It's known that PfNR undergoes an helix-coil transition upon 2'-P-AMP binding. In particular, α-helix F is shortened by two turns at its N-terminus, while the loop included between α-helix F and β-sheet 9 is correspodingly elongated by seven residues (Figure 3.22). Such a conformational changes induced by 2'-P-AMP binding have been never found in other FNRs. The same behavior has been observed in PfFNR-H286L. Interestingly, in the case of PfFNR-H286L, ligand binding was obtained only after addition of a concentration of 2'-P-AMP 3-fold higher than that required for the wild-type enzyme, consisting with the decreased affinity of this mutant for the $NADP^+$ analogue.

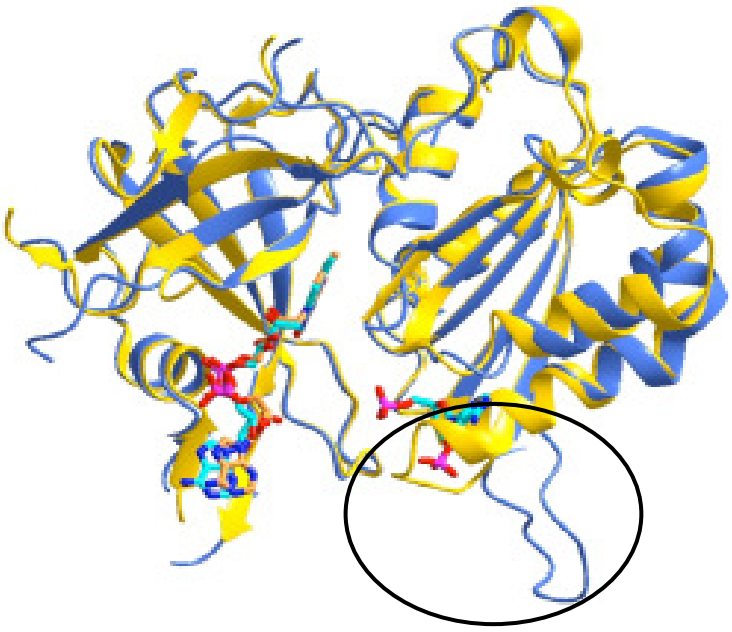

Figure 3.22. **Superimposition of PfFNR (yellow) and PfFNR-2'-P-AMP complex (blue).** In the circle is highlighted the helix-coil transition upon 2'-P-AMP binding.

On the other hand, in a manner consistent with its high affinity for the ligand (Table 3.16 and 3.17), PfFNR-H286K was easily crystallized in presence of 2'-P-AMP. Since mutation of His286 affects the affinity for 2'-P-AMP, we focused our attention on the 2'-P-AMP binding site in order to explain the possible correlations between functional and structural aspects. In the PfFNR-H286L-2'-P-AMP crystal structure the mutation mainly affect the binding mode of 2'-P-AMP, causing a displacement if its adenine end toward Tyr258, which in turn adjusts its position (Figure 3.23). Indeed the presence of Leu286 residue causes the loss of a stacking interaction between 2'-P-AMP and the protein, promoting a small sliding of the ligand toward the protein surface. In the case of PfFNR-H286K a displacement of Lys side chain occurs, likely due to the longer Lys side chain compared to His (Figure 3.23). Moreover this displacement could contribute to the destabilization of the nicotinamide-flavin interaction and thus be partially responsible for the low k_{cat} values of this mutant form (Table 3.14 and 3.15). Lys286 can also establish an electrostatic interaction with the carboxy terminus of Tyr316 that could restrict its mobility. Since displacement of the C-terminal Tyr is important for the accesibility of the nicotinamide ring of NADPH to the isoalloxazine ring of FAD, this interaction might concur to hamper the catalytic activity of PfFNR-H286K.

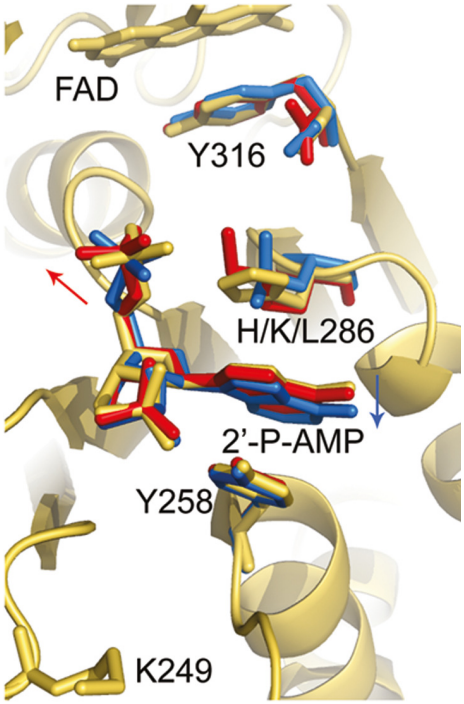

Figure 3.23. **Binding of 2'-P-AMP to wild-type and mutant PfFNR forms.** 2'-P-AMP complexes of PfFNR-H286K (red) and PfFNR-H286L (blue) superposed with that of wild-type PfFNR (yellow). The two arrows indicate the direction of sliding of the adenine ring in the Leu mutant (blue) and displacement of 5'-phosphate in the Lys mutant (red).

3.3.8 FUNCTIONAL CHARACTERIZATION OF PfFNR-K249A

In order to evaluate the possible role of Lys249 in NADPH recognition, I characterized the PfFNR-K249A mutant form. For both NADPH-$K_3Fe(CN)_6$ and NADPH-DCPIP reductase activity the k_{cat} values of this mutant are not significantly affected (220 ± 5 and 110 ± 6 e^- equiv s^{-1}, respectively). On the contrary the k_{cat}/K_m^{NADPH} values in the ferricyanide reductase reaction (0.73 ± 0.07 e^- equiv s^{-1} M^{-1}) was found to be 10-fold lower in comparison to that of the wild-type enzyme. The k_{cat}/K_m^{NADPH} ratio measured with DCPIP as substrate is only slightly affected by the Lys249Ala mutation (1.0 ± 0.13 e^- equiv s^{-1} M^{-1}). To probe the affinity of NADP(H)-binding site for its ligands, the interaction bof PfFNR-K249A with 2'-P-AMP and $NADP^+$ was investigated by inhibition and titration studies, under the same condition used for His286 mutants. The $K_i^{2'\text{-P-AMP}}$ and K_d^{NADP+} were found to be 5.4- and 8.3-fold higher compared to the wild-type enzyme, respectively. The difference absorption spectrum of the PfFNR-K249A-$NADP^+$ complex was found to be very similar to that of the complex with wt PfFNR. It's to notice that k_{cat}/K_m^{NADH} ratio of the mutant enzyme in the ferricyanide reductase reaction (0.13 ± 0.02 e^- equiv s^{-1} M^{-1}) is not differ from that of the wild-type enzyme, ruling out the possibility that the Lys249 side chain interacts with groups other than the 2'-phosphate of the substrate nucleotide.

4

DISCUSSION

Malaria is still today one of the most important infectious disease in the world, primarily due to the increasing resistance of *Plasmodium* spp. to available drugs. Indeed, new drugs against malaria parasites are urgently needed. Since FNR of *Plasmodium falciparum* (PfFNR) is a promising novel target for antimalarial therapies, I decided to look for inhibitors of PfFNR using the approach of library screening.

The results I have obtained show that *in silico* screening of virtual library is a good strategy to identify inhibitors of PfFNR. 16 compounds to which the program attributed the best score were taken into account for further analysis. In particular I determined their IC_{50} by measuring two different diaphorase activity. Four of these compounds, I19, I21, I24 and I27 turned out to be powerful inhibitors of PfFNR with an IC_{50} lower than 10 μM in the case of NADPH-$K_3Fe(CN)_6$ reductase activity, and lower than 2 μM in the case of NADPH-DCPIP reductase activity. I8 resulted to be sligthly less powerful with an IC_{50} value of about 10 μM for NADPH-DCPIP reductase activity. It should be noted that the diaphorase activity with DCPIP is the most sensitive to inhibition, probably because ferricyanide, which acts also as PfFNR inhibitor, could interfere with the interaction enzyme/inhibitor. Some of these inhibitors, I8 and I19, showed to be highly selective for Apicomplexa FNRs. I8 inhibits more efficiently *Toxoplasma gondii* FNR with respect to *Plasmodium falciparum* FNR, whereas I24 and I27 resulted to inhibit also maize root FNR. I21 compound is a known unselective inhibitor capable to inhibit a variety of NAD(H)/NADP(H)-dependent oxidoreductase. Steady-state kinetic analysis indicated that, for all the inhibitors considered, the inhibition mechanism is mixed. Unlike to that expected from the virtual library screening, the selected inhibitors doesn't act purely by competing with NADPH. However the comparison of K_i and K'_i indicates that, for all the compounds considered, the competitive inhibition component, affecting apparent k_{cat}/K_m, is predominant with respect to the that uncompetitive which affects apparent k_{cat}. Finally, the quinonic I24 turned out to act as PfFNR substrate, being rapidly oxidized from molecular oxygen with production of superoxide radical.

The screening of Prestwick Chemical Library®, performed by monitoring the NADPH-INT reductase activity of PfFNR, revealed that ebselen is active against PfFNR by acting as powerful irreversible inhibitor. For the characterization of ebselen mechanism

of action I used the enzymatic variant PfFNR-C99A which shares the same catalytic features with the wild-type form but it doesn't undergo dimerization and inactivation, simplifying the interpretation of results. Ebselen is able to inactivate PfFNR-C99A with a second order kinetic in which the rate of the process is proportional to both enzyme and inhibitor concentration, excluding a formation of reversible enzyme/inhibitor complex. Since ebselen is known to react with thiol groups by forming a selenylsulphide bond, I hypothesized that inactivation could involve Cys residues of the enzyme. For this reason I measured the second-order rate constant ($k_{ebselen}$) either at pH 8.2 or pH 7.0. Inactivation constant resulted 7-fold higher at pH 8.2 than pH 7.0 consistently with Cys side chain pK_a value of about 8. PfFNR turned out to be very sensitive to ebselen in comparison to other homologous and non-homologous FNRs. In particular *Spinacia oleracea* (spinach) FNR (SoFNR), a plant homologue of PfFNR, showed a $k_{ebselen}$ 9-fold lower than that observed for PfFNR-C99A, while *Mycobacterium tuberculosis* FprA, a ferredoxin reductase unrelated to PfFNR, is completely resistant to ebselen inhibition. The different PfFNR, SoFNR and FprA susceptibility to ebselen action suggested that a possible target of the inhibitor could be an active-site Cys, a peculiar residue of plant-like FNRs. In order to test this hypothesis, I studied the enzymatic variant SoFNR-C272S, already available in the laboratory, and PfFNR-C99A-C284S. SoFNR-C272S is resistant to ebselen, whereas PfFNR-C99A-C284S has a $k_{ebselen}$ similar to the PfFNR-C99A at pH 8.2 but 2-fold lower at pH 7.0. Effect of ebselen on PfFNR conformation have been studied by spectrofluorimetry. Enzyme-bound FAD fluorescence is quenched by the interaction between apoenzyme and fluorophore. The treatment of PfFNR-C99A with ebselen leads to a dramatic increase of FAD fluorescence indicating the dissociation of the flavin cofactor from holoenzyme. A calculation of a rate constant for FAD dissociation was made impossible because of the complexity of fluorescence time course. Nevertheless, by comparing time needed to release 50% of bound-FAD and half-life of inactivation process, the inactivation of PfFNR-C99A is faster than FAD release. This observation could be explained hypothesizing that a rapid modification of PfFNR, which causes inactivation, also destabilizes the native conformation, making the enzyme releasing FAD (with a slower kinetic). According to another hypothesis, the rapid modification of one or more Cys residues causes the loss of activity and it is followed by a slower modification of other Cys residues concomitantly to FAD release. It has been also investigated the effect of Cys284Ser mutation on FAD release promoted by ebselen. The mutation effectively slows down FAD dissociation either at pH 8.2 or pH 7.0. Differently from SoFNR, modification

of Cys284 of PfFNR seems to have a predominant role in FAD release process rather than in inactivation, suggesting that effectively FAD release and inactivation involve the modification of different Cys residues. This idea is supported also by the fact that ebselen targets two other Cys residues of PfFNR besides Cys99 and Cys284. The mechanism of ebselen inhibition resulted from this analysis could explain the inhibitory effect described also for enzymes related to plant-like FNRs, as NADPH-oxidase, cytochrome P450 reductase and NO syntase. As a matter of fact, all of these enzymes possess a conserved active-site Cys which could represent the target of ebselen action.

In 2007, the crystal structure of PfFNR has been solved as in free form and in complex with the substrate analogue 2'-P-AMP. The structure revealed that the enzyme binds the substrate in an unusual way respect to other FNRs. In particular (i) substrate binding is associated to a substantial conformational change of the binding-site, (ii) positively charged side chains interacting with 2'-phosphate group of 2'-P-AMP are lacking, (iii) His286, a residue not conserved in other FNRs in which is substituted with an aliphatic residue (Leu), could substantially contribute in the binding of both the adenilic portion and the 5'-phosphate group of the substrate.

Aim of this work is to investigate the role in catalysis of two basic residues, His286 and Lys249, located in the NADP(H)-binding site of PfFNR and far from the site where the hydride transfer (HT) between substrate and FAD bound to the enzyme occurs. In plant-like FNRs catalysis of HT occurs in two steps: first, the conversion of the ground state of NADPH in the Michaelis complex, where the nicotinamide portion of the substrate is disordered and second, the conversion to a transition state where the nicotinamide stacks onto the flavin ring according to a precise geometry. The replacement of these two residues will not affect directly the HT, rather they can influence the reductive half-reaction in two possible ways: (i) by altering the affinity for NADP(H) affecting k_{cat}/K_m^{NADPH} or (ii) by altering the orientation of nicotinamide moiety of NADP(H) affecting k_{cat}.

The replacement of His286 resulted in a complex effects depending on the replacement residue. Deletion of the imidazole group by the His286Ala mutation significantly decreases k_{cat}/K_m^{NADPH} by 15-40-fold, depending on the the electron acceptor used, and also k_{cat} is lowered to one-third of that of the wild-type enzyme. Thus, His286 seems to play a critical role not only in NADP(H) binding but also in orienting the nicotinamide portion of the bound substrate to favor HT to FAD. This conclusion is supported by 2'-P-AMP inhibition and by $NADP^+$ binding studies, where a 5-10-fold decreasing in affinity was observed.

Unexpectedly, replacement of His286 with Leu impaired the catalytic activity of PfFNR to an even greater extent than the mutation to Ala. The crystal structure of the complex PfFNR-H286L-2'-P-AMP showed a significant shift of the position of bound analogue which could explain the destabilization of the HT-competent conformation of the nicotinamide moiety. Moreover rapid kinetics studies attest that in this enzyme form the CT complexes are destabilized and HT proceeds at a rate 3.4-fold lower than in the wild-type enzyme.

Such results remark the notion that the imidazole ring of His286 establishes with NADP(H) critical contact for catalysis, which an aliphatic group cannot form.

Surprisingly, the substitution of His286 with Lys led to the lowest k_{cat}. Since PfFNR-H286K resulted to bind 2'-P-AMP and $NADP^+$ with high affinity, I concluded that this mutation specifically destabilized the HT-competent conformation of NADP(H) in the transition state. The crystal structure of the complex PfFNR-H286K-2'-P-AMP suggested that this effect could be due to a slight displacement of the pyrophosphate group of bound NADP(H), which can be transmitted to the nicotinamide moiety.

Replacement of His286 with a Gln resulted in an enzyme form that was highly active and mantained ligand binding properties similar to those of the wild-type enzyme. PfFNR-H286Q displays a k_{cat} significantly higher than that of PfFNR, due to a 1.6-fold increase in the HT rate, as shown by stopped-flow experiments. $NADP^+$ binding induced more intense spectral perturbations when bound to PfFNR-H286Q than to PfFNR, and a greater amount of CT species were observed in the case of this mutant form with respect to PfFNR during enzyme photoreduction in the presence of $NADP^+$ and during enzyme reaction with NADPH, as studied by rapid mixing. These observations indicate that the higher k_{cat} values of PfFNR-H286Q are due to a better stabilization provided by Gln, compared to His, of the HT-competent conformation of NADPH.

I have replaced also Lys249, a residue located in the NADP(H) adenylate-binding loop of PfFNR. The crystal structure of PfFNR-2'-P-AMP did not highlight interactions between this residue and the ligand (Milani *et al.*, 2007). However, I argued that Lys249 would be sufficient flexible in solution to let its side chain reach the 2'-phosphate of the bound substrate. As a matter of fact, the Lys249Ala substitution resulted in a 10-fold decrease in k_{cat}/K_m^{NADPH} with no effect on the k_{cat} of the ferricyanide reductase reaction. The role of Lys249 in binding NADP(H) was confirmed also by 2'-P-AMP inhibition and $NADP^+$ binding sudies. The slight effect of Lys249 substitution on the NADPH-DCPIP reductase reaction remains unclear, although it could be due to the fact that the rate of this reaction is

limited by the enzyme oxidative half-reaction. Moreover the Lys249Ala replacement showed no effect on the NADH-dependent activity of PfFNR, confirming that the group of NADP(H) which interacts with Lys249 side chain is indeed the 2' phosphate. As the whole, these results indicate that the positively charged side chain of Lys249 interacts with NADP(H) but it has no role in the stabilization of the HT-competent conformation of bound NADPH.

In conclusion, the two basic residues Lys249 and His286 located in the adenylate-binding subsite of PfFNR play a significant, although not essential, role in NADP(H) binding, as shown also by the pH profile in the case of His286. Moreover, while Lys249 contributes to binding of the ground- and transition-state conformations of the substrate by interacting with its 2'-phosphate, His286 plays a role also in favoring the HT-competent conformation of NADP(H) by interacting with its pyrophosphate group. This interaction is critical in orienting the nicotinamide moiety of the substrate towards the flavin ring. The hydrogen bonding potential of the His286 side chain, rather than its possible ionic character, seems to be essential for this function, since the His286Gln mutation does not impair the catalytic properties of the enzyme, and even favors CT interactions and HT, while the His286Lys replacement dramatically slows turn-over.

Since large amounts of the purified recombinant PfFNR-C99A are required to support the in-depth biochemical study and the characterization of inhibitors, I overproduced PfFNR-C99A as cleavable fusion with SUMO protein. The global yield resulted 3-fold less than the recombinant PfFNR-C99A obtained without the SUMO fusion. The major factor limiting the accumulation of the fusion protein in *E. coli* is the partial proteolytic degradation *in vivo* observed for polyHis-SUMO-PfFNR-C99A. Nevertheless this low yield is compensated by the fact that this strategy is a fast and cheap lab-scale purification procedure.

In conclusion, the peculiar features of PfFNR highligthed by functional studies of mutant forms in addition to the individuation of compounds active against this enzyme, render PfFNR an attractive target suitable for the development of antimalarial compounds.

REFERENCES

Abrahamsen M. S., *et al.*, (2004), Science 304, 441-445

Aliverti A. *et al.,* 2001 *Biochemistry* 40 14501-14508

Aliverti A. *et al.*, 2008 Arch. Biochem. Biophys. 474, 283-291

Balconi E., *et al.*, FEBS Journal, 276 (2009), 3825-3836

Balmer Y *et al.,* 2006 *Proc. Natl. Acad. Sci. USA* 103 2988-2993

Bannister L. H., *et al.*, (2003), *Journal of Cell Science* 116, 3825-3834.

Batie C.J. and Kamin H., 1984 *J. Biol.Chem.* 259 11976-11985

Bradford M. (1976), *Anal. Biochem* 72*,* 248-254.

Bisanz C. *et al.*, 2006 Biochem. J., 394 197-205

Campbell E. A. *et al.*, 2001 Cell 104 901-912

Carrillo *et al.* 2003 *Eur. J. Biochem.* 270 1900-1915

Carruthers V. B., *et al.*, (1979), *Eur J Cell Biol*. 73(2):114-23.

Couto A. S. *et al.*, 1999 *Biochem. J.* 341 629-637

Clastre M. *et al*., Exp. Parasitol. 116, 375-384

Deng Z. *et al.,* 1999 *Nat. Struct. Biol.* 6 847-853

DeRoche *et al.*,2000 *J. Cell Sci.* 113 3969-3977

Disch A. *et al.*, 1998, *Biochem J.*, 333 381-388

Foth B. J. *et al.,* 2003 *Int Rev Cytol* 224 57-110

Fleige T. *et al.*, 2010, Microbes Infect., 12, 253-262

Funes S., *et al.*, 2004 , 6 305-311

Gardner M. J. *et al.*, 2002 Nature 419, 498-509

Gardner M. J., *et al.*, 1991, Mol. Biochem. Parasitol. 44 115-123

Goodman C. D. *et al.*, 2007, Cuur. Drug Targets 8, 15-30

Goodsell, D. S., *et al.*, (1996), *J. Mol. Recognition*, 9: 1-5

Heath R. J. *et al*.,2002 *Appl. Microbiol. Biotechnol*. 58 695-703

Heinemann I. U. *et al*., 2008 Arch. Biochem. Biophys. 474, 238-251

Hopkins J. *et al.*, 1999, *Protist*, 150 283-295

Hüter A. M., *et al.*., *Parasitol. Res.*, (1989); 75 (5): 353-360

Jomaa H. *et al.*, 1995 *Science* 285 1573-1576

Karplus P. A. *et al.*, 1991 *Science* 251 60-66

Karplus P. A. *et al.*, 1994 *J. Bioenerg. Biomembr.* 26 89-99

Kohler S., *et al.*, 1997, Science, 275 1485-1489

Laemmli U. K. (1970), *Nature* 227, 680-685.

Levy C. W. *et al.*, 1999 *Nature* 398, 383-384

Maulik N., *et al.*,. (1998), *Free Radical Biology & Medicine*, Vol. 24, No. 5, pp. 869-875

McFadden G. I., *et al.*, (1999), Trends in Microbiology, 7(8) 328-333.

McFadden G. I., *et al.*, 1997, Plant. Syst. Evol. 11 (Suppl.) 264-287

Milani M., *et al.*., *J. Mol. Biol.*, (2007) 367, 501-513.

Müller A, *et al.*,. (1984), *Biochem Pharmacol.*, Oct 15;33(20):3235-9

Neuhaus H. E. *et al.*, 2000, *Annu. rev. Plant Physiol. Plant Mol. Biol.*, 51 111-140

Nickel C. *et al.,* 2006 *Antiox. Redox Signal.* 8 1227-1239

Obornik M. *et al.,* 2006, Int. J. Parasitol. 39, 1-12

Piubelli L., *et al.*,. (2000), *J. Biol. Chem. 275*, 10472-10476.

Prasad A. R. K. *et al.*, 1995, Biochem. Biophys. Re. Commun., 215 186-191

Ralph S. A. *et al.,* 2004 *Nature Reviews Microbiology* 2(3) 203-216

Rock C. O *et al.*,2002 *Biochem Biophys Res Commun* 292, 1155-1166

Roos D. S. *et al.*, 1999 *Current Opinion in Microbiology* 2 426-432

Roos D. S. *et al.*, *Phil. Trans. R. Soc. Lond*. (2002) 357, 35-46

Schewe T., (1995), *Gen. Pharmac.*, Vol.26, No. 6, pp. 1153-1169

Schwender J. *et al.,* 1996 *Biochem J.*, 316 73-80

Seeber F., 2005 *Current Pharmaceutical Design* 11 3159-3172

Seeber F. *et al.*, 2008 Trends Parasitol*.,* 24 468-478

Seeber F. *et al.*, 2010 Int. Rev. Cell Mol. Biol., 281 161-228

Sheiner L. *et al.*, 2008 Traffic 9 636-646

Siddall M. E., 1992. Hohlzylinders. *Parasitol. Today*. 8 90-91

Singh N. *et al.*, 2007, Curr. Pharm. Des. 13, 1161-1177

Surolia A., *et al.*, *Biochem. J.* (2004) 383, 401–412

Thieler H. *et al.*, (1966), *Klin wochenschr* 44, 464-467.

Thompson D. C., *et al.*, (1995), *Toxicology Letters*, 81: 141-149

Tonkin C. J. *et al.*, 2008 Traffic 9 166-175

Vollmer M. *et al.* 2001, *J. Biol. Chem.* 276 5483-5490

Waller R. F. *et al.,* 1998 *Proc. Natl. Acad. Sci. U.S.A*, 95 12352-12357

Waller R. F. *et al.*, 2000 The EMBO Journal 19 (8) 1749-1802

Wilson R. J., *et al.*, J. Mol. Biol. 261 (1996) 155-172

Yung S. *et al.*, 2003 *J. Parasitol.* 89 767-776

Zuegge J. *et al.,* 2001 *Gene* 280,19-26

ABBREVIATIONS

[Fe-S]	iron-sulfur cluster
HT	hydride transfer
E_m	mid-point potential
CT	charge transfer
IMAC	immobilized metal ion affinity chromatography
DTT	dithiothreitol
PMSF	phenylmethanesulfonyl fluoride
PVDF	polyvinylidene fluoride
DCPIP	dichlorophenolindophenol
FAD	flavin adenine dinucletide
HEPES	4-(2-hydroxyethyl)-1-piperazineethanesulfonic acid
IPTG	isopropil-β-D-thiogalactopyranoside
k_{cat}	turnover number
K_d	dissociation constant
K_m	Michaelis-Menten constant
NADPH	reduced adenine dinuocleotide phosphate
NADH	reduced nicotinamide adenine dinucleotide phosphate
2'-P-AMP	adenosin-2'-5'-diphosphate
EDTA	ethylenediaminetetraacetic acid

PUBLICATION

D. Crobu, G. Canevari, M. Milani, V. Pandini, M. A.Vanoni, M.Bolognesi, G. Zanetti and A. Aliverti, (2009) "*Plasmodium falciparum* ferredoxin-$NADP^+$ reductase His286 plays a dual role in NADP(H) binding and catalysis", *Biochemistry* 48, 9525-9533.